Manuscript prepared for Geosci. Model Dev. Discuss.
with version 2015/04/24 7.83 Copernicus papers of the LaTeX class copernicus.cls.
Date: 5 February 2016

Evaluation of an operational ocean model configuration at 1/12° spatial resolution for the Indonesian seas (NEMO2.3/INDO12)– Part 1: Ocean physics

B. Tranchant[1], G. Reffray[2], E. Greiner[1], D. Nugroho[3,4], A. Koch-Larrouy[3], and P. Gaspar[1]

[1]CLS, Ramonville Saint-Agne, France
[2]Mercator Ocean, Ramonville Saint-Agne, France
[3]IRD/LEGOS 18 av. Ed. Belin, 31401 Toulouse, France
[4]Agency of Research and Development for Marine And Fisheries, MMAF, Jakarta, Indonesia

Correspondence to: B. Tranchant (btranchant@cls.fr)

Abstract

INDO12 is a 1/12° regional version of the NEMO physical ocean model covering the whole Indonesian EEZ. It has been developed and is now running every week in the framework of the INDESO project (Infrastructure Development of Space Oceanography) implemented by the Indonesian Ministry of Marine Affairs and Fisheries.

The initial hydrographic conditions as well as open boundary conditions are derived from the operational global ocean forecasting system at 1/4° operated by Mercator Ocean. Atmospheric forcing fields (3 hourly ECMWF analyses) are used to force the regional model. INDO12 is also forced by tidal currents and elevations, and by the inverse barometer effect. The turbulent mixing induced by internal tides is taken into account through a specific parameterization. In this study we evaluate the model skill through comparisons with various datasets including outputs of the parent model, climatologies, in-situ temperature and salinity measurements, and satellite data. The biogeochemical model results assessment is presented in a companion paper (Gutknecht et al., 2016).

The simulated and altimeter-derived Eddy Kinetic Energy fields display similar patterns and confirm that tides are a dominant forcing in the area. The volume transport of the Indonesian ThroughFlow (ITF) is in good agreement with the INSTANT current meter estimates while the transport through Luzon Strait is, on average, westward but probably too weak. Compared to satellite data, surface salinity and temperature fields display marked biases in the South China Sea. Significant water mass transformation occurs along the main routes of the ITF and compares well with observations. Vertical mixing is able to modify the South and North Pacific subtropical waters salinity maximum as seen in TS diagrams.

In spite of a few weaknesses, INDO12 proves to be able to provide a very realistic simulation of the ocean circulation and water mass transformation through the Indonesian Archipelago. Work is on-going to reduce or eliminate remaining problems in the second INDO12 version.

1 Introduction

INDO12, a 1/12° regional version of the NEMO/OPA 9.0 (Madec et al.,1998) physical ocean model covering the whole Indonesian EEZ has been developed in a fully operational mode. It is now running every week in the framework of the INDESO project (Infrastructure Development of Space Oceanography). This project has been devised and funded by the Indonesian Ministry of Marine Affairs and Fisheries to support sustainable exploitation of Indonesian marine resources. The Indonesian infrastructure within this project has been designed and dimensioned for an operational system at 1/12°. Compared to ORCA12 (Global configuration at 1/12°), INDO12 includes the tide effect that induces important processes in the Indonesian region. It is easier to modify and tune the parameters in a regional configuration. Moreover, ORCA12 may benefit from the improvements of the regional configuration. INDESO actually includes the development of a series of coupled ocean models including a biogeochemical model and a fish population dynamics models covering three commercially important tuna species (skipjack, yellowfin and bigeye tunas). Results of the biogeochemical model are presented in a companion paper (Gutknecht et al., 2016) while simulations of tuna population dynamics will be discussed in a further paper. More details about the INDESO projects can be found at http://www.indeso.web.id.

The Indonesian archipelago is the only area where two major oceans, the Pacific and the Indian, are connected near the equator. An additional complicating factor comes from the internal variability associated with ENSO. The complex geometry of the coastlines, the strong tides and the seasonal reversal of monsoonal winds make it difficult to obtain a detailed and realistic representation of the ocean circulation. Numerical models of the oceanic circulation through the Indonesian archipelago have been developed and prove to be rather successful.

In this paper, we focused on the physics. A realistic modeling of the circulation in the Indonesian Archipelago helps to understand the role of the ITF at global scale. ITF carries water from the tropical Pacific into the Indian Ocean in a region where (i) the bottom bathymetry is complicated (see Fig. 1), (ii) numerous narrow straits and deep interior (semi-

enclosed) basins down to 4000 m depth (Sulawesi, Molucca and Seram Seas) exist and (iii) tidal mixing permits the transformation of incoming Pacific source waters into different water masses. Thus, vertical mixing within the Indonesian Archipelago makes substantial changes to the incoming stratified Pacific thermocline waters.

The major input of the ITF is the Mindanao Current that provides water from the upper thermocline (North Pacific Subtropical Water, NPSW) and North Pacific Intermediate Water (NPIW). This branch fills the archipelago through the Sulawesi Sea and then flows through the Makassar Strait (Gordon, 1986; Murray and Arief, 1988; Gordon and Fine, 1996). Because the Makassar strait is only 600 m deep, waters below this depth are prevented from progressing southward. About 80 % of the ITF transport is flowing through this shallow Makassar strait (mainly the thermocline waters), (Gordon et al., 2010). This branch of the ITF flows out of the archipelago through the Lombok Strait (about 20 % of the Makassar transport) or eventually reaches the Flores or Banda Seas to finally exit through Ombaï strait or Timor Passage (Gordon and Fine, 1996).

Two secondary Eastern routes exist. The first route is taken by South Pacific Intermediate Water (SPIW) going from the South Equatorial Current (SEC) through the Maluku (or Molluca) Sea and the Lifamatola Strait into the Banda Sea and further through the Ombaï Strait or the Timor Passage into the Indian Ocean. The South Pacific Subtropical Water (SPSW) from the SEC takes the second route through the Halmahera and Seram Seas and eventually joins the first eastern route waters in the Banda Sea.

Finally, an important path of the ITF is the flow through the SCS (South China Sea) and is referred as South China Sea Through-Flow (SCSTF). The cold and salty water inflow through the Luzon Strait becomes a warm and fresh water outflow through the Mindoro and Karimata straits, with a net volume transport of 2–4 Sv ($1\,\mathrm{Sv} = 10^6\ \mathrm{m^3\,s^{-1}}$), (see Qu et al., 2004).

The Indonesian archipelago is characterized by strong internal tides, which are trapped in the different semi-enclosed seas of the archipelago, inducing a strong mixing of water masses. Susanto et al. (2005) observed internal solitary waves generated in stratified water by interaction of successive semi-diurnal tidal flows with the sill south of the Lombok strait.

These waves create large vertical displacements of water masses that are important to vertical transport and the mixing of biogenic and non-biogenic components in the water column (Munk and Wunsh, 1998).

Vertical mixing within the Indonesian Seas can alter the incoming stratified Pacific thermocline waters. Salinity maximums of Pacific waters, 34.8 PSU in the North Pacific and 35.4 PSU in the South Pacific are eroded during their residence in the Indonesian Seas. The ITF waters entering into the Indian Ocean are characterized by a unique water mass associated with a unique tropical stratification with a salinity of 34.6 PSU. As a result, the tropical Indian Ocean is cooled and freshened by the ITF, (Song and Gordon, 2004, 2005). Previous studies show that vertical mixing occurs mainly in regions of sharp topography such as sills or narrow straits (Ffield and Robertson, 2008; Koch-Larrouy et al., 2007). However, the exact location of water mass transformations remain unclear (Koch-Larrouy et al., 2007). Different measurements of turbulent dissipation rates made during the INDOMIX 2010 cruise (Koch-Larrouy et al., 2015) could certainly help to increase our knowledge and understanding of vertical eddy diffusivity values for use numerical models.

To take into account internal tidal mixing, the model explicitly solves the barotropic tides. At the resolution of the model, only part of the baroclinic energy will be generated (Niwa and Hibiya, 2011). Nevertheless, how this energy will dissipate in the model remains unclear and the tidal mixing remains insufficient. To this end, an additional parameterization of tidal mixing is used to reproduce the effect of internal tides. This parameterization has especially been developed for OPA/NEMO in Indonesian Seas and gives satisfying results compared to observations (Koch-Larrouy et al., 2007, 2008 2010).

This paper compares the result of the first INDESO simulation against previous results from literature detailed above in Indonesia Seas. It is organized as follows. Section 2 describes the INDO12 configuration. Section 3 shows different model comparisons with different relevant dataset in the area. We assess INDO12 dynamics against recent scientific literature. We compare meso-scale variability and tides with altimeter data and tide gauges. Comparisons with satellite data such as SST and SSS are done. We also make comparisons with monthly gridded fields combining ARGO floats (Array for Real-time Geostrophic

Oceanography), Triangle Trans-Ocean Buoy Network (TRITON), and available conductivity-temperature-depth (CTD). We compare model volume transport with transport estimates from the INSTANT campaign. Regarding the water mass transformation in the Indonesian Seas, we compare T/S diagrams of the INDO12 simulation to the parent and to observational data, such as climatology, the recent INDOMIX 2010 cruise (Koch-Larrouy et al., 2014-AGU, 2015 in revision to Deep Sea) and instantaneous data in 2013. Finally, Sect. 4 provides a summary of the results of this work.

2 The INDO12 configuration

2.1 The NEMO ocean model

The regionalized configuration of the Indonesian Seas using OPA/NEMO model (Madec et al., 1998; Madec, 2008) in its NEMO2.3 version called INDO12 and developed at Mercator-Ocean is the circulation model used in the INDESO project. This NEMO2.3 version has already been successfully applied to the IBI (Iberian-Biscay-Ireland) area (Maraldi et al., 2013). It deals with the addition of high-frequency processes such as tide and the atmospheric pressure forcing. Specific numerical schemes such as time-splitting, non-linear free surface (Levier et al., 2007) and open boundary algorithms have been implemented or improved. Specific physical parameterizations for regional modeling have been added such as GLS turbulence model (Umlauf and Burchard, 2003) including wave impact and logarithmic bottom friction. In addition, the vertical mixing induced by internal tides is taken into account using the parameterization of Koch-Larrouy et al. (2007) by artificially enhancing the vertical viscosity and the diffusion coefficients. In semi-enclosed seas, an approximate value of 1.5 $cm^2.s^{-1}$ for eddy diffusivity has been estimated by Koch-Larrouy et al. (2007). Note that this background diffusivity is of the same order of magnitude as that used by Jochum and Potemra (2008).

The domain covers 20° S–25° N and 90–144° E (Fig. 1) and includes the entire EEZ (Exclusive Economic Zone) of Indonesia. The horizontal grid is an extraction of the global

ORCA grid at 1/12° developed at Mercator Ocean. It is a quasi-regular grid over the Indonesian area and with a mesh approximately equal to 9 km. In the vertical direction, the model uses a partial step z coordinate (Barnier et al., 2006). The vertical grid is spread over 50 levels and has a depth-dependent resolution (1 m at surface to 450 m at the bottom). In the first 10 m, the layer thickness is less than 2 m, then rise to about 10 m at a depth of 50 m.

The bathymetry used in this configuration is based on ETOPO2V2g (2′) and GEBCO (1′) and has been interpolated on the NEMO grid without any smoothing. Due to missing foreshore in the model, a minimal threshold value of 7 m depth has been fixed. The bathymetry has been locally modified by a hand editing mainly in the straits and passages where the sill depths have a major interest and constrain the transports. As in Metzer et al. (2010), we report sill values on Table 1 and compare them to scientific literature. Note that correct sill depths are essential for proper model simulation (Gordon et al., 2003a). Without these changes, the outflow passages were quite incorrect with most of the flow going through the Lombok strait instead flowing through the Ombaï strait and the Timor passage. Note that the INDO12 configuration is coupled 'online' to the biogeochemistry model PISCES (see Gutknecht et al., 2016).

2.2 External forcings

Atmospheric forcing fields come from the European center (ECMWF) and have a high frequency (3 h). "Bulk" formulae from CORE are used to model the atmosphere–ocean interface (Large and Yeager, 2004). The surface atmospheric pressure forcing is also explicitly considered.

This configuration includes explicit tidal forcing. INDO12 has geopotential tidal forcing for M2, S2, N2 and K2 (the four largest semi-diurnal constituents) and for K1, O1, P1 and Q1 (the four largest diurnal constituents). As in Maraldi et al. (2013), two long-period tides Mf and Mm and one non-linear constituent (compound tides) M4 are also added. These 11 tidal constituents come from the astronomical forcing TPX0.7 dataset(Egbert and Erofeeva, 2002) are used to force open boundaries.

A monthly runoff climatology is built with data on coastal runoffs and 99 major rivers from Dai and Trenberth (2002) and prescribed with a flux formulation. In addition, two important rivers (Mahakam and Kapuas on Borneo Island) with large enough rates (class 3) were added to this database.

The penetration light scheme used in this simulation is based on a 4-bands decomposition of the light. 54 % of the solar radiation is trapped in the surface layer with an extinction depth of 0.35 m and the other part is decomposed following the red, green and blue wavelengths (Jerlov, 1968). The climatological chlorophyll values, required to calculate the absorption coefficients, were deduced from the global 1/4° input file built from the monthly SeaWifs climatological data (McClain et al., 2004).

The longest available period to force the INDO12 model and to achieve the operational target set by the INDESO project was the Mercator-Ocean Global Ocean Forecasting System at 1/4° (PSY3V3R3) (Lellouche et al., 2013), data from 2007 to 2013. Therefore, the INDO12 simulation starts on the 3rd January 2007 with initial conditions coming from PSY3V3R3 run started three months before from a Levitus climatology (WOA 2005), see (Antonov et al., 2006).

These conditions include temperature, salinity, currents and Sea Surface Height (SSH). Open boundary conditions (OBCs) are located on a relaxation band of 10 grid points ($\sim 1°$) and come from daily output of the Global Ocean Forecasting System at 1/4° of Mercator Ocean.

3 INDO12 assessment

In order to evaluate the quality of the INDO12 simulation, several diagnostics were performed on different variables such temperature, salinity and currents. Our performance analysis confronts the model results to the distinct available datasets. The first year (2007) of the simulation is considered as the model spin-up phase. Consequently, only the 2008–2013 simulated period is assessed.

3.1 The mean circulation

As noted by Ueki el al. (2003), the NGCC (New Guinea Coastal Current) exhibits a seasonal variability correlated to the monsoonal wind variation with a North-East wind stress during the Boreal winter and a South-West wind stress during the Boreal summer. It flows northward usually at the surface and is intensified during the Boreal summer. It flows southeastward during the boreal winter (see Fig. 2). The New Guinea Coastal Under Current (NGCUC) flows steadily northwestward during the whole year in the sub-surface thermocline layer (100–300 m) with an intensification during the boreal summer (see Fig. 3).

In the Pacific region (Fig. 2), the intensity of SEC and (North Equatorial Counter Current) NECC increase during boreal winter, and are weaker during Boreal summer. The SEC and NECC are closely linked to the ITCZ (Inter Tropical Convergence Zone). They are stronger from August to December and weaker from March to May (see McPhaden et al., 1998).

Between the surface and $\sim$ 100 m depth, the seasonal variability is well represented in the major exit passages of the Lombok Strait, Ombaï Strait and Timor Passage with a maximum velocity (maximum transport) during the SEM (South East Monsoon) (Sprintall et al., 2009).

In the SCS, the circulation at the surface is cyclonic during the boreal winter and weakly anti-cyclonic during boreal summer, see (Fig. 2).

In the Indian Ocean, the Eastward surface current, the SJC (South Java Current) flows along the Indian Ocean coast of Sumatra and Java only during the NEM (North East Monsoon). During the SEM, the SJC is mostly in the same direction as the westward flowing ITF (Sprintall et al., 2010), which is well reproduced in our simulation. The deeper South Java UnderCurrent (SJUC) flows also along the coast (400–800 m) in the model. It clearly seems that it is driven by Kelvin waves as mentioned by Sprintall et al. (2010) since it flows mainly eastward whatever the monsoon period.

3.2 EKE

In order to describe the mesoscale and the eddy variability, the mean Eddy Kinetic Energy (EKE) is calculated. The EKE calculation is performed over the last three years (2010–2013) of the INDO12 simulation and compared to altimetry data (AVISO products), see Fig. 4.

Saraceno et al. (2008) point out the difficulty of representing coastal processes with conventional altimeter data. It is mainly due to intrinsic difficulties such as corrections applied to the altimeter data near the coast (e.g., the wet tropospheric component, high-frequency oceanographic signals, tidal corrections, etc.). The Indonesian Seas are no exception to the rule due to the presence of numerous islands and an active atmospheric convection during the monsoons. In addition, in the equatorial band (5° S–5° N) the geostrophic approximation is not valid since the Coriolis force vanishes.

Except in coastal regions, the EKE from INDO12 and the EKE derived from altimeter data have the same patterns for strongest values. They are localized along the Vietnam coast, near the Luzon strait (Kurushio intrusion in the SCS) and all along the Java coast (upwelling signature). In the INDO12 simulation, stronger values are found in all the straits and in the main exits (Lombok, Ombaï and Timor). As in Castruccio et al. (2013), large EKE values are also found within the Indonesian Seas, Celebes Sea, Flores Sea, Molluca Sea and the southern part of the Banda Sea. In the Pacific, Halmahera and Mindanao eddies as well as the NGCC also show a strong signature in the EKE field. On both sides of Luzon strait, the EKE from INDO12 exhibits weaker values than the EKE derived from altimeter data (AVISO). These weak EKE values corroborates the weak inflow as mentioned in the section 3.6.

3.3 Tides

The four primary tidal components, namely M2, S2, K1, and O1 are found to be the major components that drive tidal forcing in the Indonesian Seas (Ffield and Robertson, 2008; Kartadikaria et al., 2011). In this section, we present only two primary tidal components, M2 and K1, the largest amplitude semidiurnal and diurnal constituents. Kartadikaria

et al. (2011) have fully described the evolution of the M2 and the K1 tides in the Indonesian Seas. They show that (i) the propagation of the K1 is simpler than that of the M2 component (ii) and the K1 amplitude is smaller than that of M2. Here, the K1 and M2 constituents are compared to a hydrodynamic model of the barotropic tides constrained by satellite altimetry FES2012 (Carrere et al., 2012; Stammer et al., 2014). The INDO12 tidal sea surface elevation amplitude and phases were calculated as a complex amplitude using standard harmonic analysis applied to the sea surface height. Differences of tidal elevation between satellite altimeter data (TOPEX/POSEIDON, JASON 1 and JASON2) at crossover locations and models (INDO12 and FES2012) are shown in Fig. 5. For the M2 constituent, FES2012 is closest to the observations excepted in the SCS. On the contrary, for the K1 constituent, INDO12 is closest to the observations except in the SCS and along the Australian coast. Differences of tidal elevation between tides gauges (circles) and models and are also given in the same figure. Closer to the coast, the discrepancy between tide gauges and INDO12 is larger than between tide gauge and FES2012. This can be attributed to the lack of resolution along the coast in INDO12 compared to the finite element FES2012.

Figure 6 shows a power-spectrum analysis of hourly SSH from Tide gauges and from simulated moorings. As in Castruccio et al. (2012), at low frequencies (period larger than 10 days), the model is in very good agreement with the observations. The spectral analysis shows that SSH fluctuations depict the same peaks at the dominant tidal frequencies, the diurnal (O1 and K1) and semidiurnal (M2 and S2). The same intensity is found in the model and in the observations. It confirms that tides are a dominant forcing in the area, and that the tidal current is dominated by the diurnal (O1 and K1) and semidiurnal (M2 and S2) frequencies. Non-linear constituents are represented by additional peaks at the higher harmonics that contain less energy in the model than the observations. As mentioned in Ffield and Robertson (2008), model errors are mainly due to a topography, stratification, resolution, and tidal forcing. Indeed, tide gauges are very close to the coast where the INDO12 model is less able to well represent non-linear processes. Finally, non-linear tides seems also to have more energy in the model near the East of Sumatra coast (Fig. 6a) than in the Pacific (Fig. 6c).

3.4 SSS: comparisons with Aquarius and Argo monthly data

Due to the important role of the low salinity surface layer waters (coming from the SCS southward throughflow) on the ITF (Gordon et al., 2012), it is important to assess the SSS fields of INDO12.

3.4.1 Aquarius data

We used the Aquarius Level 3 sea surface salinity (SSS) standard mapped image data that contains gridded 1° spatial resolution SSS averaged over one month. This particular data set is the Monthly sea surface salinity product for version 3.0 of the Aquarius data set, which is the official second release of the operational data from AQUARIUS/SAC-D mission. A summary of improvements to this new version of the Aquarius data is available.

For the previous version (V2.0), the estimated error for (monthly mean) was around 0.3–0.4 PSU (Lagerloef et al., 2013). A recent paper of Menezes et al. (2014) shows that rms difference between the Aquarius (7 day Level-3 product version 2.0) and Argo is about 0.28 PSU in the tropical eastern basin of the Indian ocean [5–20° S; 90–140° E], i.e. in a region where the fresh ITF is spread westward. In addition, in a very recent paper, Tang et al. (2014) show that the monthly RMS difference with respect to Argo between 40° S and 40° N for all Aquarius SSS data products (V2.0) can be reduced to below 0.2 PSU with some limitations.

3.4.2 JAMSTEC data

As in Tang et al. (2014), we use a monthly gridded data set of global oceanic salinity on $1^\circ \times 1^\circ$ grid processed and delivered by the Japan Agency for Marine-Earth Science and Technology (JAMSTEC) (Hosoda et al., 2008). This product is derived from the use of the optimal interpolation (OI) method that builds the gridded fields from ARGO floats, TRITON, and available CTD.

The salinity values at 10 m depth from INDO12 are compared with the first level of JAMSTEC salinity at 10 dbar ($\sim$ 10 m depth).

The advantage of the monthly Aquarius data is the spatial coverage. Monthly JAMSTEC data does not cover the Indonesian Seas due to a lack of in-situ data.

3.4.3 Results

For both datasets, a negative bias exist in the Pacific region (Fig. 7) except near the Mindanao loop current where a positive bias exist mainly in winter. It is more pronounced with the Aquarius dataset. We show that the probability density function (pdf) of SSS misfit is biased and non-symmetric which corroborates the fact that processes and/or water masses into the Pacific and Indian oceans are different. The biases relative to each dataset are consistent for the same coverage except in the northern Pacific (above 10° N) where Aquarius SSS data are probably polluted by strong RFI (Radio Frequency Interference), see Kim et al. (2014) and Le Vine et al. (2014). They are quite similar but stronger for Aquarius. In the Indian Ocean, a positive bias exists just after the ITF exit. It becomes negative near the Eastern Gyral Current (EGC) that flows eastward near 15° S. In the upper ocean, a strong salinity front exists between the fresh water from the ITF in the South Equatorial Current (SEC) and the salty subtropical waters (Menezes et al., 2013). Note also that the ITW joins the SEC and spreads westward in the Indian Ocean by advection and diffusion (Gordon et al., 1997).

Un-correlated biases near the west-Sumatra coast are located in the vicinity of many islands that could pollute the Aquarius signal. The RMSD (Root Mean Square Deviation) between JAMSTEC and INDO12 in this region is higher (Fig. 8) than the RMSD between Aquarius and INDO12.

A strong negative bias (too fresh) exists in the South China Sea (SCS) which is more (in winter) or less (in summer) important depending on the season (not shown here). It could be related to an E-P bias in the ECMWF precipitation flux where the model simulation of precipitation is particularly poor over Indonesia, (see Kidd et al., 2013; Dee et al., 2011). In a recent paper, Zeng et al. (2014) argue that the smaller LST is a plausible cause of the freshening in 2012. In our model, the too strong freshening could also be due to a too weak transport at Luzon.

A positive bias exists in the southern tropical Indian Ocean except during April/May/June when the bias tends to be negative. There is a seasonal variation of the bias into the Pacific. In the interior domain, the bias is less pronounced and there is not a seasonal signal.

RMSD and correlations in SSS between Aquarius and INDO12 are quite similar to those between JAMSTEC and INDO12 in the Pacific and Indian oceans. In the interior domain, RMSD/correlation (Fig. 8) between Aquarius and INDO12 are larger/smaller in the Java Sea (monsoon variability), in the Gulf of Thailand and in the Taiwan strait (probably due to land contamination).

A region in the Indian Ocean (95° E–15° S) is characterized by a smaller correlation between both INDO12 and both dataset. It is certainly due to a systematic bias in the boundary conditions. This bias can be related to a lesser accuracy of MDT (Mean Dynamic Topography) (Rio et al., 2013) in the South Indian Ocean. Indeed, the MDT is involved in the process of SLA (Sea Level Anomalies) data assimilation in the parent ocean forecasting system. From Fig. 9 (left), we show that in the Indian Ocean, the three main opposite differences (statistically significant) between the two datasets (uncorrelated biases) are in the Timor Sea, in the Andaman Sea and on the west-coast of Sumatra. These differences can be partially explained by the salinity interpolation errors shown on Fig. 9 (right) since the maximums are found at the same locations. The Timor Sea is mainly located on the continental shelf which would results in the large interpolation errors due to the absence of ARGO floats. An uncorrelated bias exists at the entrance of the Indonesian domain, in the Celebes Sea and corresponds to the maximum of the salinity interpolation errors.

Due to the lack of JAMSTEC data in the interior domain, it is difficult to conclude on the quality of Aquarius data. Nevertheless, comparisons in the SCS (Sect. 3.5.3) have shown that the INDO12 model is fresher than the in-situ data at surface which is corroborated here with Aquarius data.

3.5 SST: comparisons to AMSR-E and Argo monthly data

The SST of the Indonesian Seas is of major interest to air–sea interaction at regional and global scales (see for example Sanchez et al., 2008). This is due largely to the convection process.

3.5.1 AMSR-E data

We use the SST (Sea Surface Temperature) data retrieved from observations of the satellite microwave radiometer Advanced Microwave Scanning Radiometer on board EOS (AMSR-E). The advantage of using microwave data instead of infrared data is that the clouds' influence can be neglected. For this study, in order to be close to the horizontal resolution ($1^\circ \times 1^\circ$) of JAMSTEC (see above), we use the night-time monthly averages SST map ($1^\circ \times 1^\circ$) from the AMSR-E version 7 SSTs (see www.remss.com). The TAO array shows AMSR-E to have very small biases ($-0.03\,^\circ$C) and STD ($0.41\,^\circ$C) (Gentemann et al., 2010).

3.5.2 JAMSTEC data

As in Tang et al. (2014), we use a monthly gridded data set of global oceanic temperature on $1^\circ \times 1^\circ$ grid processed and delivered by the Japan Agency for Marine-Earth Science and Technology (JAMSTEC) (Hosoda et al., 2008). This product is derived from the use of the optimal interpolation (OI) method that builds the gridded fields from ARGO floats, TRITON, and available CTD.

The temperature values at 10 m depth from INDO12 are used to compare with the first level of JAMSTEC temperature at 10 dbar (~ 10 m depth).

3.5.3 Results

Compared to both datasets, the SST in the model is too warm overall (Fig. 10). The SST bias is larger in the SCS where the influence of SCSTF is important (Qu et al., 2006) through the Luzon Strait. Positive biases are of similar amplitude between the two datasets

and are mainly located in the Pacific region. This increased the confidence in the positive bias in the SCS and corroborates the negative bias in the SSS. A too weak deep-water overflow in the Luzon strait can also explained this large bias. Zhao et al. (2014) show that enhanced mixing in the SCS is a key process responsible for the density difference between the Pacific and SCS, which in turn drives the deep circulation in the Luzon Strait.

There is only one important region where the INDO12 SST is significantly too cold, it is in the southern part of the INDO12 domain, i.e. in the southern tropical Indian Ocean. The negative bias relative to JAMSTEC is larger than the bias relative to AMSR-E as it is for the RMSD (Fig. 11). It is localized in the Eastern Gyral Current (EGC) that flows eastward near 15° S, i.e., in the same region where a positive SSS bias exist (see previous section). In the Indonesian Archipelago, the SST bias relative to AMSR-E is slightly positive except in the Flores and Molluca Seas and in the Timor passage where the bias is slightly negative. The Timor passage is the only region where a non-correlated bias exists between the two datasets (Fig. 12a). It still corresponds to the maximum of the temperature interpolation errors (Fig. 12b) in JAMSTEC. The temporal correlation (Fig. 11) is rather high everywhere and consistent between two datasets. Only one region located near the Halmahera eddy and along the SEC seems less correlated.

3.6 Volume transport (ITF and SCSTF)

The Indonesian ThroughFlow (ITF) flow along three main routes (Sprintall et al., 2004) and a good representation is given in (Gordon et al., 2012; Fig. 1).

The main western route is the flow taken by the North Pacific Subtropical Water coming from the North Equatorial Current (NEC) via the Mindanao Current through the Celebes Sea, along the Makassar Strait, into the Flores Sea and the Lombok or the Ombaï Strait into the Indian Ocean. In the South part of the Makassar Strait, only the upper thermocline waters can flow southward into the Flores and Banda Seas due to the Dewakang sill (650 m).

The second path is taken by the South Pacific sub-thermocline water, going from the South Equatorial Current (SEC) through the Maluku Sea and the Lifamatola Strait into

the Banda Sea and further through the Ombaï Strait or the Timor Passage into the Indian Ocean. The Lifamatola Strait, at 1940 m, regulates the flow of deep Pacific water into the interior Indonesian Seas. Talley and Sprintall (2005) show that the IIW (Intermediate Indonesian Water) attains most of its characteristics immediately downstream of the Lifamatola Strait as a result of the diapycnal mixing of the intermediate Pacific Ocean water masses. They also estimate a large total southward transport (~ 3 Sv). Below 1250 m, the average volume transport through Lifamatola during INSTANT (about 1.5 years between January 2004 and July 2005) was 2.5 ± 1.5 Sv (van Aken et al., 2009). It is a fairly robust number with an uncertainty of ~ 5 % below 1250 m which it is not the case above 1250 m with an uncertainty that exceeds 50 % (Gordon et al., 2010). Finally, the total transport measured by INSTANT (El-Niño period) below 200 m is 1.1 Sv. In our simulation (2008–2013), the total transport is quite null and flows northward (1.6 ± 3 Sv) below 1250 m with no inter-annual variability. Above 1250 m, the net inflow is southward and varies with ENSO (El-Niño–Southern Oscillation). It is stronger during La-Niña and weaker during El-Niño. From Fig. 13, we show that the upper thermocline waters flow southward. The flow is northward between 400 and 1400 m. The only deep water flowing southward is located below 1400 m with a maximum near 1700 m depth in spite of the presence of an opposite flow on the eastern side of the strait. It is a strong discrepancy with measurements and can be attributed to the bathymetry located upstream of the strait or to the open boundary conditions.

The SPSW (South Pacific Subtropical Water) from the SEC takes the third route through the Halmahera and Seram Seas and joins the second route waters in the Banda Sea.

We consider the transport through the three major outflow passages of Lombok, Ombaï and Timor to determine the ITF transport estimates as in Sprintall et al. (2009). Table 2 gives absolute values of transport in each straits and total transport for the 2008–2013 simulated period compared to the INSTANT estimates (Gordon et al., 2010). The total value measured by INSTANTS (15 Sv) is stronger than in the model (12.4 Sv). This might be attributed to the prescribed ocean forcing fields given by the Mercator-Ocean Global Ocean Forecasting System at 1/4° (PSY3V3R3) and to an inaccurate bathymetry in the important straits. Also,

INSTANT estimates and simulated INDO12 volume transports are not calculated over the same period with different ENSO signals.

Significant transport variability during the INSTANT period is linked to the ENSO and to the IOD (Indian Ocean Dipole) phenomena (Sprintall et al., 2009; Gordon et al., 2008; Van Sebille et al., 2014). The INSTANT estimates reveal also inter-annual fluctuation, see Table 1 of Gordon et al. (2010). Nevertheless, Sprintall and Revelard (2014) argue that the 3 year time series alone is not sufficient to comprehensively resolve the interannual signal. In the INDO12 simulation, Fig. 14 shows that a strong inter-annual variability exists and is more or less pronounced depending both on locations and on competing ENSO/IOD events. In 2008 and 2013, ENSO and IOD signals were generally weak but the simulated ITF transports were among the largest in the period, particularly in Ombaï and Timor straits. In 2011 and 2012, there is no ENSO event and a positive IOD, and it gives quite equivalent total transports. In 2009, the only El-Niño of the simulation period takes place and no IOD event; consequently, the weakest ITF transport of the period occurs that year. In 2010, La Niña coincides with a negative IOD. In this case, the ITF transport is reduced with the weakest transport in Ombaï and the negative IOD seems to prevail. In a recent paper, Sprintall and Revelard (2014) argue that Indian Ocean dynamics likely win out over the Pacific Ocean dynamics during concurrent ENSO and IOD events. Indeed, the ITF transport variability would be linked both to spatial patterns of SLA and to zonal wind stress anomalies. During concurrent La Niña and negative IOD events (e.g. 2010), a stronger SSH signature exists in both Pacific and Indian Oceans with higher SLA throughout the Indonesian Archipelago. In the same time, a westerly winds anomaly (September-December) in the tropical Indian Ocean would lead reverse the upper layer ITF transport (Lombok, Ombaï and Timor) via downwelling Kelvin waves. Whereas during a solo La Niña event, only a slight SLA imbalance exists in the Pacific latitude bands around 5–10°. This leads to off-equatorial Rossby waves which result in an increase in Timor volume transport as suggested by Mc Clean et al., 2005. Note that during the INDO12 simulation (2008-2013), there was no such event.

In order to better compare the relative transport in each of the three exit straits, we give the ratio with regard to the total mean transport volume and compare them with INSTANT estimates (Gordon et al., 2010), see Table 2.

On the one hand, this ratio (%) in the INDO12 simulation is very close to the INSTANT estimates values for Lombok strait, but on the other hand this ratio is lower for the Ombaï strait and stronger in the TIMOR passage. However, if we compare the absolute volume transport (Sv) in the Timor passage, it compares favorably to INSTANT estimates, whereas the Ombaï strait transport is substantially weaker than INSTANT estimates, see also Fig. 14. In a recent paper, Oke et al. (2013) found the same kind of differences with a longer reanalysis.

The South China Sea ThroughFlow (SCSTF) affects the near surface flow in the Makassar Strait (Qu et al., 2006). It leads to the subsurface maximum in the southward current of the Makassar Strait. Gordon et al. (2003b) have shown that the intrusion of freshwater from the SCS effectively inhibits the Makassar Strait surface water from freely flowing southward. As a consequence, the Indonesian throughflow (ITF) heat transport is significantly reduced during the northeast monsoon season. The Luzon strait is the major pathway between the SCS and the Pacific Ocean. The LST (Luzon Strait Transport) is estimated to be westward and about -4 ± 5.1 Sv at 120.75° E, (Hsin et al., 2012). In the INDO12 simulation, this volume transport is westward and around -0.4 Sv. This leads to a lack of salt water coming from the Pacific Ocean. Recent studies suggested different ways of improvement. Hulburt et al. (2011) shows that simulations are very sensitive to model resolution and to the accuracy of the topography and sill depths within the narrow straits in the Philippine archipelago. More recently, Zhao et al. (2014) show that the transport of the deep circulation increases with diapycnal diffusivity in the deep SCS and Luzon Strait.

3.7 Water masses transformation

In this section, we deal with the water masses transformation in the Indonesian Seas. We compare INDO12 T–S diagrams with WOA 2013 climatology and with parent model (PSY3) in several sub-basins along the pathways within the Indonesian archipelago as in Koch-Larrouy et al. (2007), see Fig. 15. T–S diagrams of parent and INDO12 models are

compared to INDOMIX CTD data in July 2010 (Koch-Larrouy et al., 2015). Model and climatology (WOA2009) T–S diagrams are also compared to instantaneous data (WOD 2013) on both sides of Luzon Strait.

In addition to these T–S diagrams, we highlight different biases into the MLD that give indications on upper ocean stratification.

3.7.1 Comparisons with parent model and WOA2013 climatology

Water masses from the INDO12 simulation (averaged all over the period from 2008 to 2013) are compared with those of the WOA 2013 climatology (Boyer et al., 2013) and with those of the parent model (PSY3V3R3) in main areas of water mass transformation, see Fig. 15.

At the main entrance, the Mindanao Current drives the North Pacific water characterized by a salinity maximum (34.8 PSU), the North Pacific Subtropical Water (NPSW) and a minimum of 34.2 PSU (North Pacific Intermediate Water, NPIW). Coming from the North Pacific, the NPSW is saltier in the INDO12 simulation than in the WOA 2013 climatology. The NPIW and the surface water are fresher (Fig. 16a).

South Pacific Subtropical Waters (SPSW) enter also into the Indonesian Seas and are characterized by a salinity maximum around 35.45 PSU. Compared to the WOA 2013 climatology, the SPSW in the INDO12 simulation are slightly too warm at the surface and at the sub-surface (Fig. 16b).

Because open boundary conditions are close to the North and South Pacific Waters properties, the INDO12 and parent model (PSY3V3R3) differ from WOA 2013 climatology in the same way.

When comparing TS diagram in the interiors seas between the regional model that includes tidal mixing to the parent model that does not include any additional mixing, we find that the tidal mixing of the SPSW has occurred before entering the Banda Sea (Fig. 17a,b,c). In the Banda, Seram and Timor regions, the North and the South Pacific subtropical salinity maximums are strongly attenuated in the INDO12 simulation. It is not the case for the parent simulation.

In particular, the SPSW salinity maximum is strongly eroded from its entrance in the Halmahera Sea and vanishes already in the Seram Sea as noted by Koch-Larrouy et al. (2007). The tidal mixing strongly improves the water masses. However, there are still some biases between the climatology and the INDO12 simulation that could come from observed biases at the entrance of the domain.

During their residence in the Indonesian archipelago, the incoming Pacific waters are transformed to produce a unique water mass associated with a unique homohaline tropical stratification (34.58 PSU, below 20 °C), see T/S diagrams in the Timor region on Fig. 18. In the Timor and Banda regions, at the surface there is a strong freshening compared to the climatology. But comparisons do not take into account the inter-annual variability and some disparities exist depending on the year (Figs. 8 and 12). This freshening is not observed at the entrance of the Indonesian domain (NPW). It is due to the Surface fresh water coming from the Java Sea water that represents the major freshwater input (70 %, Koch-Larrouy et al., 2008). Moreover, a too strong freshening is observed in the model (see Sects. 3.7.3 and 3.4.1). Surface water of Makassar strait and Flores Sea are lower than 33.8 PSU. It is certainly due to a lack of salt water coming from the Pacific Ocean, see Sects. 3.6 and 3.7.3. This behavior is enhanced in 2011 (Fig. 18) when the LST is the strongest (-1.19 Sv) in the INDO12 simulation. The effect of a too strong mixing in the Banda Sea (Fig. 17b) can also enhance the too strong freshening at the surface.

Comparing the model over a limited period of time to a climatology that suffers from a lack of data to properly represent inter-annual variability and regional rapid changes between the seas of the archipelago, is an imperfect exercise to validate the model. Fortunately, the INDOMIX cruise occurred during the period of our simulation, providing a unique dataset to validate the model.

3.7.2 Comparisons with CTD from INDOMIX campaign

The INDOMIX cruise (July 2010, Koch-Larrouy et al., 2015) recovers in-situ measurements in one of the most energetic section for internal tides through the Halmahera Sea and the Ombaï strait. Classical fine-scale CTD/LADCP measurements have been performed

together with micro-structure measurements at five locations, two at the entrance of the Halmahera Sea (S0, S1), two in the Halmahera Sea (S2, S3), one in the Banda Sea (S4) and two (S5a/S5b) in the Ombaï strait (Fig. 19).

Koch-Larrouy et al. (2007) argued that the vertical mixing due to internal tides of the SPSW occurs mainly within the Halmahera and Seram Seas before entering the Banda Sea.

In the following section, we compared instantaneous INDOMIX profiles (July 2010) to parent model (daily mean) and to the INDO12 simulation (hourly instantaneous) profiles. We see that before entering the Halmahera Sea (Fig. 20/S0), a maximum of salinity is present, and is in better agreement with observations in INDO12 simulation compared to the parent model. The combined effect of the horizontal resolution and explicit tides has a crucial role. The INDO12 model exhibits a zigzag shape profile that suggests intense lateral mixing probably produces by the explicit tides.

In the Halmahera strait (Fig. 20/S1), the salinity maximum has already been reduced both in the observations and in the simulations. The vertical mixing seems to be too strong in the INDO12 simulations since the mixed layer is too salty and the lower thermocline is warmer and fresher. It is in better agreement with observation than the parent model that exhibits strong salinity a maximum.

At the S2 and S3 locations in the Halmahera Sea (Fig. 20), T/S profiles display temperature and salinity structure with "wiggles" and step features in the thermocline (more pronounced than in S1 location). Ffield and Robertson (2008) found a similar temperature fine structures associated to the straits, the shallow shelves, and the proximity of the shelf-slope boundary in the Indonesian Seas. This phenomenon seems to be amplified during the windy JJA Southeast Monsoon time period when the upper thermocline is less stratified, especially during La Niña years that which corresponds to July 2010. They associated this temperature fine structure with internal wave activity that can be a precursor to turbulent vertical mixing. It is not clear if the horizontal and vertical resolution of INDO12 prevents the reproduction of this wave activity or if it occurs slightly away of the station location.

As in S1, the mixing seems too strong since the mixed layer is too salty and the lower thermocline is warmer and fresher.

INDO12 T/S diagrams compare quite well with the INDOMIX data in the Banda Sea (S4). It is the result of the mixing and the advection of water masses coming from the Java and the Flores Seas. In the Ombaï strait (S5), INDO12 fits very well with the INDOMIX data below the pycnocline. The NPIW (density 26.5) seems to be well mixed in the observations, certainly by isopycnal mixing but it is no the case in the INDO12 simulation where the NIPW signature is still present.

Finally, all T/S diagrams in the interior domain show that the parent model has definitively not enough efficient vertical mixing and that a higher resolution model including explicit tides is needed to mix correctly Pacific waters in the Indonesian Archipelago.

It is also interesting to know where are located the most important bias and errors in the vertical. This gives an additional indication about the upper ocean stratification. In Fig.21(a,b,c,d), most of the salinity biases for INDO12 show two significant maximums, a negative bias in the mixed layer (0-50 m) and a positive bias at 150-200 m depth. The model is fresher than the observations in the lower thermocline where salty waters from SPSW penetrate into the Indonesian Seas. Moreover, this twice as large for S0 (Fig.21a) as for S1, S2 and S3 (Fig21b,c,d). As previously mentioned, this indicates that an excessively strong mixing occurs in the Halmahera strait and the Seram Sea. The Parent model show a systematic negative bias over the whole water column for salinity with two pronounced peaks near the SPSW penetration and in the mixed layer. Except in S0 where two peaks exist, maximum errors (RMSD) are found below the mixed layer depth (near 100 m), i.e in the upper thermocline. In S4 (Fig21e), a positive salinity bias exists only in the mixed layer depth for INDO12 whereas in S5 (Fig21.e) a slight salty bias exists over the whole water column with a maximum in the upper thermocline. For temperature, except in S0, INDO12 temperature at S1, S2 and S3 are too warm (negative bias) down to 300 m depth, i.e in the lower thermocline. Below 600 m depth, a cold bias exists (positive) with a gradually increase at S2 (Fig21c). In S4 (Banda Sea), it is quite different since two opposite biases exist in the lower and upper thermocline and no more significant positive bias for deep layers. As

previously mentionned, the NIPW signature is present at S5 location (Fig.21f) with a larger bias near 800 m depth but with also a larger variability since the RMSD is larger.

3.7.3 Comparisons to in-situ data in the SCS (October–December 2013)

Comparisons of INDO12 simulations and WOA 2009 climatology collocated with real in-situ profiles (WOD 2013) have been done in on both sides of the Luzon strait for the autumn 2013 (October-December). We focus on the SCS region that is connected to the Pacific Ocean through the Luzon strait in the northern part. In the southern part of the basin, the region links with the Java Sea through the Karimata Strait, and with the Sulu Sea through mainly through the Mindoro Strait. The fresh SCS water entering the Java Sea through the Karimata Strait inhibits the warm surface water from the Pacific flowing southward in the Makassar Strait during the boreal winter (Gordon et al., 2003b; Qu et al., 2006; Tozuka et al., 2007). As the Makassar throughflow amounts to 80 % of the total ITF, the SCS effect is a major contributor to the overall variability of the ITF vertical structure. Whereas that the Karimata transport is mostly seasonal (Fang et al., 2010), the circulation of the SCS demonstrates an inter-annual variation related to the ENSO. Gordon et al. (2012) suggest that the building of a "freshwater plug" in the western Sulawesi Sea (via the Sibutu passage) during prolonged El Niño periods inhibits the Mindanao surface layer injection into the Makassar Strait. On the contrary, during La Niña the "freshwater plug" is dissipated which leads to the penetration of surface water from the tropical Pacific Ocean.

On both sides of the Luzon strait (Figs. 22), the INDO12 model tends to be fresher mainly at the surface. This indicates that not enough Pacific waters enter into the SCS and it corroborates the too weak volume transport of thermocline waters observed at the Luzon strait, see Sect. 3.6. The INDO12 model (Fig. 22a) show NPSW and NPIW already shown previously (Fig. 16a) and it is quite close to observations. In the SCS (Fig. 22b), the INDO12 model is too fresh. T/S profiles shows that vertical mixing acts by disrupting the NPSW but in a too strong way by the INDO12 model. The SCS region is known as a place where the representation and the localization of internal waves and their associated vertical mixing is

still difficult to quantify. Recently Alford et al. (2015) made new measurements in the Luzon strait to better understand the formation of the world's strongest known internal waves.

As in the previous section, the bias and the RMSD of salinity and temperature are shown on both sides of the Luzon strait, see Fig 23a,b. On the Eastern side of Luzon strait (Fig.23a), salinity biases are mainly located in the first 50 meters and are significant for the INDO12 model only. After the Luzon Strait, salinity biases are larger and spread deeper down to 200 m for the INDO12 model only. The climatology seems to have no significant biases and RMSD of salinity is equivalent for the climatology and the INDO12 model. For temperature biases, opposite biases exist for the INDO12 models and in a lesser extend for the WOA 2009 climatology. From too cold (positive bias) on the Eastern side of the Luzon strait, the sea surface temperature becomes too warm (negative bias) on its western side and systematically too cold from the upper thermocline to the bottom. It is not the case for the WOA 2009 climatology that is systematically too cold (positive bias) over the whole water column.

4 Summary

The INDESO operational system has been designed to monitor the evolution of the circulation, biogeochemistry and fish population dynamics within the Indonesian Seas. Practically, INDESO addresses the needs of the Balitbang KP for a complete new oceanographic centre in Perancak, Bali, from the building to the computer systems, the satellite antenna, and the transfer of expertise to the Indonesian experts. Since mid-September 2014, the entire system (Ocean, Biogeochemistry and Fish population dynamics) is fully operational in Perancak (see http://www.indeso.web.id) and delivers 10 day forecast/two weeks hindcast on a weekly basis. In order to validate the ocean physic, the INDO12 model based on NEMO 2.3 was integrated during 7 years (2007–2013).). This period is fairly short but it was the longest operational period able to be constrained by the global ocean forecasting system at 1/4° (PSY3V3R3).

Overall, the mean circulation induced by the main equatorial and coastal currents (i.e., NGCC, SEC, NECC, SJC etc.) is well reproduced by the INDO12 ocean model. Except in coastal regions, the EKE from INDO12 and the EKE derived from altimeter data share the same patterns. On both sides of the Luzon strait, the weak EKE values from INDO12 corroborates the weak SCSTF. The model estimations of complex elevation amplitudes (amplitude and phase) agree reasonably well with the TOPEX/POSEIDON, JASON 1 and JASON2 crossover observations, with better agreement for the diurnal constituents K1 than the semidiurnal constituent M2. A power-spectrum analysis of the hourly SSH from Tide gauges and from simulated moorings shows that the model is in very good agreement with the observations at low frequencies. It confirms that tides are a dominant forcing in the area, and that the tidal current is dominated by the diurnal (O1 and K1) and semidiurnal (M2 and S2) frequencies. The non-linear constituents (higher harmonics) contain less energy in the INDO12 model than the observations due to a lesser accuracy of non-linear processes near the coast. Compared to two different SST datasets, one from space (AMSR-E) and one from an in-situ product (JAMSTEC), an overall warm bias exists and it is quite equivalent between the two datasets. It is also consistent with the SSS bias (fresh bias). Stronger values of the SST biases are located in the SCS. Only one region is too cold, it is in the southern tropical Indian Ocean. In the Indonesian Archipelago, it is difficult to discern a general trend due to the large interpolation errors and the lack of data.

We need to improve the large discrepancy in the SCS both for SSS and SST that are influenced both locally by the monsoons and remotely by the SCSTF/ITF. As mentioned by Qu et al. (2009), despite the considerable progress that has been made in the past years, our understanding of the SCSTF is far from complete. They also pointed out that Mindoro strait can play a significant role by shifting the NEC bifurcation (Mindanao Eddy) and then the Kurushio intrusion. This enhances the importance to have realistic Pacific open boundary conditions which influences the position of the Mindanao Eddy. We show that monthly SSS from space (Aquarius V3.0) and from an in-situ product (JAMSTEC) are quite consistent. This shows that the INDO12 model SSS is too low in the SCS and it corroborates the too weak volume transport of thermocline waters observed in the Luzon strait. A positive

bias exists in the southern tropical Indian Ocean (95° E–15° S) where a smaller correlation between both INDO12 and both the observation datasets exist. It is certainly due to a systematic bias in the Eastern boundary conditions related to a lesser accuracy of the MDT.

Zhao et al. (2014) show that the enhanced mixing in the SCS is a key process responsible for the density difference between the Pacific and the SCS, which in turn drives the deep circulation in the Luzon Strait.

The relative volume transport in the three major outflow passages in the INDO12 simulation is very close to one calculated from the INSTANT estimates. There is still an imbalance between the Timor strait (too strong) and the Ombaï strait (too weak). The LST is Westward but still too weak. It could be due to the model resolution and to the accuracy of the topography in the Philippine archipelago as suggested by Hulburt et al. (2011). In a recent study, Zhao et al. (2014) argue that an increase of the diapycnal diffusivity in the deep SCS and the Luzon Strait enhances the transport of the deep circulation. A strong discrepancy exists between the few existing measurements and the INDO12 simulation in the Lifamatola strait. As for the LST, it might be attributed to the bathymetry located upstream of the strait but also to the prescribed ocean forcing fields given by the Operational Ocean Forecasting System at 1/4° (PSY3V3R3). This could also explain the fact that the total transport in the INDO12 model is lower. Note also that the INSTANT estimates and the simulated INDO12 volume transports are not calculated over the same period (different ENSO/IOD signals).

The model is forced by explicit tides, which are able to generate part of the total internal tides energy. Accordingly to Niwa and Hibiya (2011), only 60 % of the baroclinic energy can be generated with a 1/12° model. The model is also forced by an existing parameterization of the mixing (Koch-Larrouy et al., 2007). The resulting vertical mixing is able to erode the South and North Pacific subtropical waters salinity maximum as seen in the TS diagrams. Compared to climatologies, the inflow coming from North Pacific seems too salty for NPSW and too fresh in surface for NPIW, the inflow coming from South Pacific seems too salty and too warm in surface and sub-surface. The SPSW salinity maximum is strongly eroded from its entrance in the Halmahera Sea and vanishes in the Seram Sea. A too fresh surface

water mass coming from the SCS throughflow and also a too strong mixing in the Banda Sea could explain a strong surface freshening into the Timor water masses. Nevertheless, an inter-annual variability exists depending on the year.

Compared to data collected during the INDOMIX cruise, an excessively strong vertical mixing occurs in the INDO12 model into the Halmahera Sea which is not able to reproduce the observed "wiggles" and step features in the thermocline. On the other hand, TS profiles fit quite well in the Banda Sea and the Ombaï strait. Finally, all T/S diagrams in the Indonesian Archipelago show that the parent model has definitively not enough efficient vertical mixing and that a higher resolution model including explicit tides is needed to mix correctly the Pacific waters in the Indonesian Archipelago.

Compared to WOD (2013) in-situ data, the INDO12 model tends to be fresher mainly at the surface in the SCS. This confirms what it has been previously observed in the SCS with SSS and SST satellite data. It is certainly the consequence of a too weak transport of Pacific water at the Luzon strait.

Different possible ways of improving the INDO12 model can be suggested. A recent and better tidal forcing (FES 2012), see Carrere and Lyard (2012) could improve tidal currents. New boundary conditions from the 1/12° global ocean forecasting model are also planned and should be more consistent (same horizontal resolution and same bathymetry). In addition, the new 1/12° global ocean forecasting system will start from the WOA 2013 climatology. This new initialization should improve the deeper T/S biases found in the Indonesian Archipelago where there is not enough observation data to efficiently constrain the model with the data assimilation system. They could give us some indications of the Mindanao Eddy influence on the LST. Next developments should also include an improved bathymetry in major straits (entrance and exit). A specific study on vertical mixing induced by internal waves is necessary in order to improve the current tidal mixing parameterization.

Finally, although the ITF has a major impact on the global ocean circulation and climate variability, there are still too few measurements in the Indonesian Archipelago.

Code and Data Availability

The INDO12 configuration is based on the NEMO2.3 version developed at Mercator Ocean. All specificities included in the NEMO code version 2.3 are now freely available in the recent version NEMO 3.6, see the NEMO web site http://www.nemo-ocean.eu. The INDO12/NEMO2.3 configuration and all the input files used in the present paper are available upon request (please contact benoit.tranchant@cls.fr).

World Ocean Database and World Ocean Atlas are available at https://www.nodc.noaa.gov. Aquarius data L3 (V3.0) data are available at http://podaac.jpl.nasa.gov/dataaccess. AMSR data are produced by Remote Sensing Systems and sponsored by the NASA Earth Science MEaSUREs DISCOVER Project and the NASA AMSR-E Science Team. Data are available at www.remss.com. JAMSTEC data are available at http://www.jamstec.go.jp/ARGO/argo_web/prod/oi_prs_e.html

Acknowledgements. This work was funded by the INDESO project. The authors thank Nathalie Verbrugge, Loren Carrere and Antoine Delepoulle for fruitful discussions and for sharing data. Comments by two anonymous reviewers and the editor greatly improved the paper. The author would like to thank Marc Lucas for his valuable help in correcting the manuscript's english.

References

Alford, M. H., Peacock, T., MacKinnon, J. A., Nash, J. D., Buijsman, M. C., Centuroni, L. R., Chao, S.-Y., Chang, M.-H., Farmer, D. M., Fringer, O. B., Fu, K.-H., Gallacher, P. C., Graber, H. C., Helfrich, K. R., Jachec, S. M., Jackson, C. R., Klymak, J. M., Ko, D. S., Jan S., Johnston, T. M. S., Legg, S., Lee, I.-H., Lien, R.-C., Mercier, M. J., Moun, J. N., Musgrave, R., Park, J.-H., Pickering A. I., Pinkel, R., Rainville, L., Ramp, S. R., Rudnick, D. L., Sarkar, S., Scotti, A., Simmons, H. L., St Laurent, L. C., Venayagamoorthy, S. K., Wang, Y.-H., Wang, J., Yang, Y. J., Paluszkiewicz, T., and Tang, T.-Y. D.: The formation and fate of internal waves in the South China Sea, Nature, 521, 65–69, doi:10.1038/nature14399, 2015.

Antonov, J. I., Locarnini, R. A., Boyer, T. P., Mishonov, A. V.,and Garcia, H. E.: World Ocean Atlas 2005, Vol. 2: Salinity, in: NOAA Atlas NESDIS 62, edited by: Levitus, S., US Government Printing Office, Washington, DC, 182 pp., 2006.

Barnier, B., Madec, G., Penduff, T., Molines, J.-M., Treguier, A.-M., le Sommer, J., Beckmann, A., Biastoch, A., Boning, C., Dengg, J., Derval, C., Durand, E., Gulev, S., Remy, E., Talandier, C., Theetten, S., Maltrud, M., McClean, J., and de Cuevas, B.: Impact of partial steps and momentum advection schemes in a global circulation model at eddy permitting resolution, Ocean Dynam., 56, 543–567, doi:10.1007/s10236-006-0082-1, 2006.

Boyer, T. P., Antonov, J. I., Baranova, O. K., Coleman, C., Garcia, H. E., Grodsky, A., Johnson, D. R., Locarnini, R. A., Mishonov, A. V., O'Brien, T. D., Paver, C. R., Reagan, J. R., Seidov, D., Smolyar, I. V., and Zweng, M. M.: World Ocean Database 2013, edited by: Levitus, S. and Mishonov, A., NOAA Atlas NESDIS 72, 209 pp., 2013.

Carrère, L., Lyard, F., Cancet, M., Guillot, A., and Roblou, L.: FES2012: a new global tidal model taking advantage of nearly 20 years of altimetry, in: Proceedings of meeting, 20 years of altimetry, Venice-Lido, Italy, 24–29 September 2012, 6 pp., 2012.

Castruccio, F. S., Curchitser, E. N., and Kleypas, J. A.: A model for quantifying oceanic transport and mesoscale variability in the Coral Triangle of the Indonesian/Philippines Archipelago, J. Geophys. Res.-Oceans, 118, 6123–6144, doi:10.1002/2013JC009196, 2013.

Dai, A. and Trenberth, K. E.: Estimates of freshwater discharge from continents: Latitudinal and seasonal variations, J. Hydrometeorol., 3, 660–687, 2002.

Dee, D. P., Uppala, S. M., Simmons, A. J., Berrisford, P., Poli, P., Kobayashi, S., Andrae, U., Balmaseda, M. A., Balsamo, G., Bauer P., Bechtold, P., Beljaars, A. C. M., van de Berg, L., Bidlot, J., Bormann, N., Delsol, C., Dragani, R., Fuentes, M., Geer, A. J., Haimberger, L., Healy, S. B., Hersbach, H., Holm, E. V., Isaksen, L., Kallberg, P., Kohler, M., Matricardi, M., McNally, A. P., Monge-Sanz, B. M., Morcrette, J.-J., Park, B.-K., Peubey, C., de Rosnay, P., Tavolato, C., Thepaut, J.-N., and Vitart, F.: The ERA-Interim reanalysis: configuration and performance of the data assimilation system, Q. J. Roy. Meteor. Soc., 137, 553–597, doi:10.1002/qj.828, 2011.

Egbert, G. D. and Erofeeva, S. Y.: Efficient inverse modeling of barotropic ocean tides, J. Atmos. Ocean. Tech., 19, 183–204, 2002.

Fang, G., Susanto, R. D., Wirasantosa, S., Qiao, F., Supangat, A., Fan, B., Wei, Z., Sulistiyo, B., and Li, S.: Volume, heat, and freshwater transports from the South China Sea to Indonesian seas in the boreal winter of 2007–2008, J. Geophys. Res., 115, C12020, doi:10.1029/2010JC006225, 2010.

Ffield, A. and Robertson, R.: Temperature finestructure in the Indonesian Seas, J. Geophys. Res., 113, C09009, doi:10.1029/2006JC003864, 2008.

Gentemann, C. L., Wentz, F. J., Brewer, M., Hilburn, K. A., and Smith, D. K.: Passive microwave remote sensing of the ocean: an overview, in: Oceanography from Space, revisited, edited by: Barale, V., Gower, J. F. R., and Alberotanza, L., Springer, Heidelberg, 13–33, 2010.

Gordon, A. L.: Oceanography of the Indonesian Seas and their throughflow, Oceanography, 18, 14–27, doi:10.5670/oceanog.2005.01, 2005.

Gordon, A. L., Giulivi, C. F., and Ilahude, A. G.: Deep topographic barriers within the Indonesian Seas, in: Physical Oceanography of the Indian Ocean during the WOCE Period, editetd by: Schott, F., Deep-Sea Res. Pt. II, 50, 2205–2228, 2003a.

Gordon, A. L., Susanto, R. D., and Vranes, K.: Cool Indonesian throughflow as a consequence of restricted surface layer flow, Nature, 425, 824–828, doi:10.1038/nature02038, 2003b.

Gordon, A. L., Sprintall, J., Van Aken, H. M., Susanto, R. D., Wijffels, S., Molcard, R., Ffield, A., Pranowo, W., and Wirasantosa, S., The Indonesian throughflow during 2004–2006 as observed by the INSTANT program, Dynam. Atmos. Oceans, 50, 115–128, doi:10.1016/j.dynatmoce.2009.12.002, 2010.

Gordon, A. L., Huber, B. A., Metzger, E. J., Susanto, R. D., Hurlburt, H. E., and Adi, T. R.: South China Sea throughflow impact on the Indonesian throughflow, Geophys. Res. Lett., 39, L11602, doi:10.1029/2012GL052021, 2012.

Gutknecht, E., Reffray, G., Gehlen, M., Triyulianti, I., Berlianty, D., and Gaspar, P.: Evaluation of an operational ocean model configuration at $1/12^\circ$ spatial resolution for the Indonesian seas – Part 2: Biogeochemistry, Geosci. Model Dev. Discuss., submitted, 2015.

Hsin, Y.-C., Wu, C.-R., and Chao, S.-Y.: An updated examination of the Luzon Strait transport, J. Geophys. Res., 117, C03022, doi:10.1029/2011JC007714, 2012.

Hurlburt, H. E., Metzger, E. J., Sprintall, J., Riedlinger, S. N., Arnone, R. A., Shinoda, T., and Xu., X.: Circulation in the Philippine Archipelago simulated by 1/12° and $1/25^\circ$ Global HYCOM and EAS NCOM, Oceanography, 24, 28–47, doi:10.5670/oceanog.2011.02, 2011.

Jerlov, N. G.: Optical oceanography, American Elsevier Publ. Co., Inc., New York, 194 p., 1968.

Jochum, M., and J.T. Potemra: Sensitivity of tropical rainfall to Banda Sea diffusivity in the Community Climate System Model. J. Climate, 21, 6445–6454

Kartadikaria, A. R., Miyazawa, Y., Varlamov, S. M., and Nadaoka, K.: Ocean circulation for the Indonesian seas driven by tides and atmospheric forcings: comparison to observational data, J. Geophys. Res., 116, C09009, doi:10.1029/2011JC007196, 2011.

Kidd, C., Dawkins, E., and Huffman, G.: Comparison of precipitation derived from the ECMWF operational forecast model and satellite precipitation datasets, J. Hydrometeorol., 14, 1463–1482, doi:10.1175/JHM-D-12-0182.1, 2013.

Kim, S.-b., Lee, J.H., de Matthaeis, P., Yueh, S., Hong, C.S., Lee, J.-H. and Lagerloef, G.: Sea surface salinity variability in the East China Sea observed by the Aquarius instrument, J. Geophys. Res. Oceans, 119, 7016–7028, doi:10.1002/2014JC009983, 2014.

Koch-Larrouy, A., Madec, G., Bouruet-Aubertot, P., Gerkema, T., Bessières, L., and Molcard, R.: On the transformation of Pacific Water into Indonesian throughflow water by internal tidal mixing, Geophys. Res. Lett., 34, L04604, doi:10.1029/2006GL028405, 2007.

Koch-Larrouy, A., Atmadipoera, A., Van Beek, P., Madec, G., Aucan, J., Lyard, F., Grelet, J., and Souhaut, M.: Estimates of tidal mixing in the Indonesian archipelago from multidisciplinary INDOMIX in-situ data, Deep-Sea Res. I, 106, 136-153, doi:10.1016/j.dsr.2015.09.007, 2015.

Koch-Larrouy, A., Morrow, R., Penduff, T., and Juza, M.: Origin and mechanism of Subantarctic Mode Water formation and transformation in the Southern Indian Ocean, Ocean Dynam., 60, 563–583, 2010.

Lagerloef and the Aquarius team: Aquarius Salinity Validation Analysis, Aquarius Project Document: AQ-014-PS-0016, 18 February 2013.

Large, W. and Yeager, S.: Diurnal to decadal global forcing for ocean and sea-ice models: the data sets and ux climatologies. CGD Division of the National Center for Atmospheric Research, NCAR Technical Note, NCAR/TN-460+STR, 2004.

Lehodey, P., Senina, I., and Murtugudde, R.: A spatial ecosystem and populations dynamics model (SEAPODYM) modeling of tuna and tuna-like populations, Prog. Oceanogr., 78, 304–318, 2008.

Lellouche, J.-M., Le Galloudec, O., Drévillon, M., Régnier, C., Greiner, E., Garric, G., Ferry, N., Desportes, C., Testut, C.-E., Bricaud, C., Bourdallé-Badie, R., Tranchant, B., Benkiran, M., Drillet, Y., Daudin, A., and De Nicola, C.: Evaluation of global monitoring and forecasting systems at Mercator Océan, Ocean Sci., 9, 57–81, doi:10.5194/os-9-57-2013, 2013.

Levier, B., Tréguier, A. M., Madec, G., and Garnier, V.: Free surface and variable volume in the NEMO code, MERSEA IP report WP09-CNRS-STR03-1A, 47 pp., 2007.

Le Vine, D. M., de Matthaeis, P.,Ruf, C.S., and Chen, D.D.: Aquarius RFI detection and mitigation algorithm: Assessment and examples, IEEE Trans. Geosci. Remote Sens., 52(8), 4574–4584, 2014.

Madec, G.: NEMO ocean engine, Note du Pole de modélisation, Institut Pierre-Simon Laplace (IPSL), France, No 27 ISSN No 1288–1619, 2008.

Madec, G., Delecluse, P., Imbard, M., and Lévy, C.: OPA 8.1 Ocean General Circulation Model reference manual, Note du Pole de modélisation, Institut Pierre-Simon Laplace (IPSL), France, No 11, 91 pp., 1998.

Maraldi, C., Chanut, J., Levier, B., Ayoub, N., De Mey, P., Reffray, G., Lyard, F., Cailleau, S., Drévillon, M., Fanjul, E. A., Sotillo, M. G., Marsaleix, P., and the Mercator Research and Development Team: NEMO on the shelf: assessment of the Iberia–Biscay–Ireland configuration, Ocean Sci., 9, 745–771, doi:10.5194/os-9-745-2013, 2013.

McClain, C. R., Feldman, G. C., and Hooker, S. B.: An overview of the SeaWiFS project and strategies for producing a climate research quality global ocean bio-optical time series, Deep-Sea Res. Pt. II, 51, 5–42, 2004.

McClean, J. L., D. P. Ivanova, and J. Sprintall: Remote origins of interannual variability in the Indonesian Throughflow region from data and a global parallel ocean program simulation, J. Geophys. Res., 110, C10013, doi:10.1029/2004JC002477, 2005.

McPhaden, M. J., Busalacchi, A. J., Cheney, R., Donguy, J. R., Gage, K. S., Halpern, D., Julian, M. Ji, P., Meyers, G., Mitchum, G. T., Niiler, P. P., Picaut, J., Reynolds, R. W., Smith, N., and Takeuchi, K.: The Tropical Ocean-Global Atmosphere observing system: A decade of progress, J. Geophys. Res., 103, 14169–14240, 1998.

Menezes, V. V., Phillips, H. E., Schiller, A., Domingues, C. M., and Bindoff, N. L., Salinity dominance on the Indian Ocean Eastern Gyral current, Geophys. Res. Lett., 40, 5716–5721, doi:10.1002/2013GL057887, 2013.

Metzger, E. J., Hurlburt, H. E., Xu, X., Shriver, J. F., Gordon, A. L., Sprintall, J., Susanto, R. D., and van Aken, H. M.: Simulated and observed circulation in the Indonesian Seas: 1/12° global HYCOM and the INSTANT observations, Dynam. Atmos. Oceans, 50, 27–300, 2010.

Munk, W. and Wunsch, C.: Abyssal Recipes II: energetics of tidal and wind mixing, Deep-Sea Res., 45, 1976–2000, 1998.

Niwa, Y. and Hibiya, T.: Estimation of baroclinic tide energy available for deep ocean mixing based on three-dimensional global numerical simulations, J. Oceanogr., 67, 493–502, doi:10.1007/s10872-011-0052-1, 2011.

Oke, P. R., Griffin, D. A., Schiller, A., Matear, R. J., Fiedler, R., Mansbridge, J., Lenton, A., Cahill, M., Chamberlain, M. A., and Ridgway, K.: Evaluation of a near-global eddy-resolving ocean model, Geosci. Model Dev., 6, 591–615, doi:10.5194/gmd-6-591-2013, 2013.

Qu, T., Kim, Y. Y., Yaremchuk, M., Tozuka, T., Ishida, A., and Yamagata, T.: Can Luzon Strait Transport play a role in conveying the impact of ENSO to the South China Sea?, J. Climate, 17, 3643–3656, 2004.

Qu, T., Yan, D., and Hideharu, S.: South China Sea throughflow: a heat and freshwater conveyor, Geophys. Res. Lett., 33, L23617, doi:10.1029/2006GL028350, 2006.

Rio, M. H., Guinehut, S., and Larnicol, G.: New CNES-CLS09 global mean dynamic topography computed from the combination of GRACE data, altimetry, and in situ measurements, J. Geophys. Res., 116, C07018, doi:10.1029/2010JC006505, 2011.

Sanchez Gomez, E., Cassou, C., Hodson, D. L. R., Keenlyside, N., Okumura, Y., and Zhou, T.: North Atlantic weather regimes response to Indian-western Pacific Ocean warming: a multi-model study, Geophys. Res.Lett., 35, L15706, doi:10.1029/2008GL034345, 2008.

Saraceno, M., Strub, P. T., and Kosro, P. M.: Estimates of sea surface height and near-surface alongshore coastal currents from combinations of altimeters and tide gauges, J. Geophys. Res., 113, C11013, doi:10.1029/2008JC004756, 2008.

Shriver, J. F., Richman, J. G., and Arbic, B. K.: How stationary are the internal tides in a high-resolution global ocean circulation model?, J. Geophys. Res.-Oceans, 119, 2769–2787, doi:10.1002/2013JC009423, 2014.

Song, Q., Gordon, A. L., and Visbeck, M.: Spreading of the Indonesian throughflow in the Indian Ocean, J. Phys. Oceanogr., 34, 772–792, doi:10.1175/1520-0485(2004)0342.0.CO;2, 2004.

Sprintall, J. and Revelard, A.: The Indonesian throughflow response to Indo-Pacific climate variability, J. Geophys. Res.-Oceans, 119, 1161–1175, doi:10.1002/2013JC009533, 2014.

Sprintall, J., Wijffels, S., Gordon, A. L., Ffield, A., Molcard, R., Susanto, R. D., Soesilo, I., Sopaheluwakan, J., Surachman, Y., and van Aken, H. M.: A New International Array to Measure the Indonesian Throughflow: INSTANT, EOS Transactions, 85, 369–376, 2004.

Sprintall, J., Wijffels, S. E., Molcard, R., and Jaya, I.: Direct estimates of the Indonesian Throughflow entering the Indian Ocean: 2004–2006, J. Geophys. Res., 114, C07001, doi:10.1029/2008JC005257, 2009.

Sprintall, J., Wijffels, S. E., Molcard, R., and Jaya, I.: Direct evidence of the South Java Current sustem in Ombai Strait, Dynam. Atmos. Oceans, 50, 140–156, 2010.

Sprintall, J., Gordon, A. L., Koch-Larrouy, A., Lee, T., Potemra, J. T., Pujiana, K., and Wijffels, S. E.: The Indonesian seas and their role in the coupled ocean-climate system, Nat. Geosci., 7, 487–492, doi:10.1038/ngeo2188, 2014.

Stammer, D., Ray, R. D., Andersen, O. B., Arbic, B. K., Bosch, W., Carrère, L., Cheng, Y., Chinn, D. S., Dushaw, B. D., Egbert, G. D., Erofeeva, S. Y., Fok, H. S., Green, J. A. M., Griffiths, S., King, M. A., Lapin, V., Lemoine, F. G., Luthcke, S. B., Lyard, F., Morison, J., Müller, M., Padman, L., Richman, J. G., Shriver, J. F., Shum, C. K., Taguchi, E., and Yi, Y.: Accuracy assessment of global barotropic ocean tide models, Rev. Geophys., 52, 243–282, doi:10.1002/2014RG000450, 2014.

Susanto, R. D., Gordon, Q., and Zheng, A. L.: Upwelling along the coasts of Java and Sumatra and its relation to ENSO, Geophys. Res. Lett., 28, 8, 1599–1602, 2001.

Susanto, R. D., Mitnik, L., and Zheng, Q.: Ocean internal waves observed in the Lombok Strait, Oceanography, 18, 80–87, doi:10.5670/oceanog.2005.08, 2005.

Talley, L. D. and Sprintall, J.: Deep expression of the Indonesian throughflow: Indonesian intermediate water in the South Equatorial Current, J. Geophys. Res., 110, C10009, doi:10.1029/2004JC002826, 2005.

Tang, W., Yueh, S. H., Fore, A. G., Hayashi, A., Lee, T., and Lagerloef, G .: Uncertainty of Aquarius sea surface salinity retrieved under rainy conditions and its implication on the water cycle study, J. Geophys. Res.-Oceans, 119, 4821–4839, doi:10.1002/2014JC009834, 2014.

Tozuka, T., Qu, T., and Yamagata, T.: Dramatic impact of the South China Sea on the Indonesian Throughflow, Geophys. Res. Lett., 34, L12612, doi:10.1029/2007GL030420, 2007.

Ueki, I., Kashino, Y., and Kuroda, Y.: Observation of the current variations off the New Guinea coast including the 1997–1998 El Nino period and their relationship with Sverdrup transport, J. Geophys. Res., 108, 3243, doi:10.1029/2002JC001611, 2003.

Umlauf, L., and Burchard, H.,: A generic length-scale equation for geophysical turbulence models. J. Marine Res. 61, 235–265, doi::10.1357/002224003322005087, 2003.

Van Sebille, E., Sprintall J., Schwarzkopf, F. U., Sen Gupta, A., Santoso, A., England, M.H., Biastoch, A., Böning, C. W., Pacific-to-Indian Ocean connectivity: Tasman leakage, Indonesian Throughflow, and the role of ENSO, J. Geophys. Res.-Oceans, 119, 1365-1382,doi::10.1002/2013JC009525, 2014.

Van Aken, H. M. and Brodjonegoro, I. S.: IndraJaya, the deep-water motion through the Lifamatola passage and its contribution to the Indonesian throughflow, Deep-Sea Res. Pt. I, 56, 1203–1216, 2009.

Zeng, L., Liu, W. T., Xue, H., Xiu, P., and Wang, D.: Freshening in the South China Sea during 2012 revealed by Aquarius and in situ data, J. Geophys. Res.-Oceans, 119, 8296–8314, doi:10.1002/2014JC010108, 2014.

Zhao, W., Zhou, C., Tian, J., Yang, Q., Wang, B., Xie, L., and Qu, T.: Deep water circulation in the Luzon Strait, J. Geophys. Res.-Oceans, 119, 790–804, doi:10.1002/2013JC009587, 2014.

Table 1. Sill depths (m) of the key straits and passages in the Indonesian seas from the scientific literature and those used in INDO12.

Straits or passages	Observed estimate	INDO12
Inflow passages		
Sanhigihe Ridge (divides Pacific Ocean and Sulawesi Sea)	1350[a]	1250
Makassar Strait (Dewakang sill)	680[a]	675
Halmahera Sea Passages	580[a]	551
Lifamatola Passage	1940[b]	1950
Outflow passages		
Lombok strait	300[a]	200
Strait between Alor and Atauro Islands (upstream of Ombaï strait)	1450[d]	1400
Wetar Strait (upstream of Ombaï strait)	2450[c]	2050
Sumba Strait (north of Sumba Island)	900[d]	800
Savu Strait (connection between Savu Sea and Indian ocean)	1150[d]	1100
Timor passage (southern end)	1890[d]	1800

Source for sill depths: [a] Gordon et al. (2003a), [b] van Aken et al. (1988), [c] Sprintall et al. (2010), [d] Sprintall et al. (2009).

Table 2. Mean volume transport in the ITF (Sv and Ratio) for Lombok strait, Ombaï strait and Timor passages. Mean values from INSTANT (2004–2006) and from the INDO12 simulation (2008–2013).

Straits	INSTANT (2004–2006)		INDO12 (2008–2013)	
	Sv	%	Sv	%
Lombok	2.6	17.3	2.07	16.7
Ombai	4.9	32.7	2.76	22.2
Timor	7.5	50	7.58	61.1
Total	15		12.41	

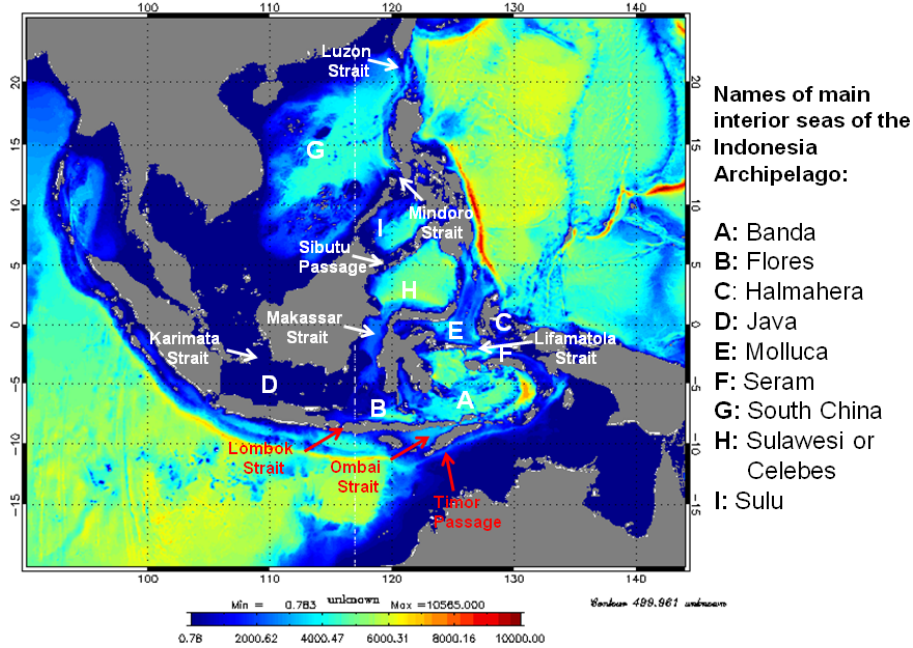

Figure 1. Bathymetry (in meters) of the INDO12 configuration (latitudes: 20° S–25° N and longitudes: 90–145° E) based on ETOPOV2g/GEBCO1 + in-house adjustments in straits of major interest. Three ITF exits are indicated in red. Main straits/passages are indicated in white.

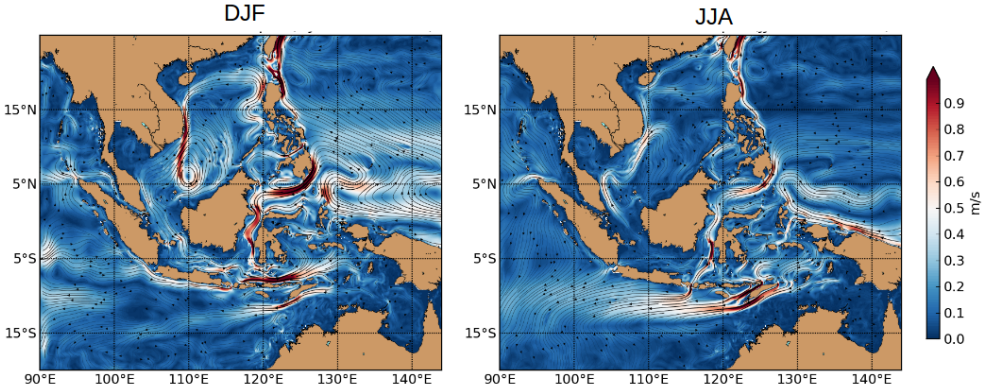

Figure 2. Mean circulation at surface (16 m depth) during boreal winter or DJF (left) and boreal summer or JJA (right) during the 2008–2013 period.

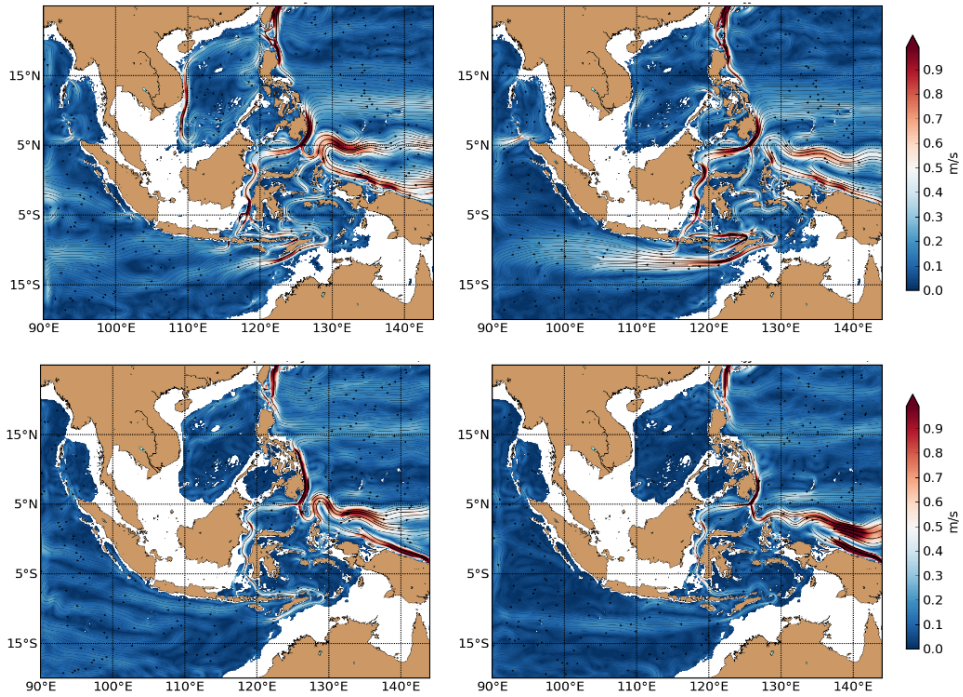

Figure 3. Mean circulation at 100 m (up) and 300 m (bottom) during boreal winter or DJF (left) and boreal summer or JJA (right) during the 2008–2013 period.

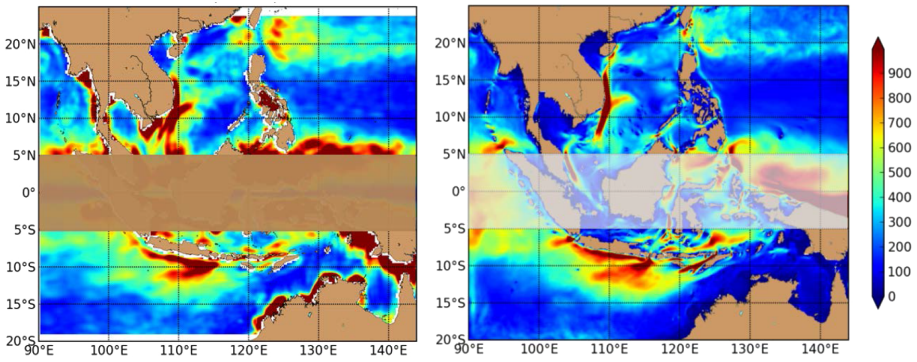

Figure 4. Mean EKE ($m^2.s^{-2}$) derived from altimetric data (AVISO products) (left) from INDO12 (right) for 2010–2013 period. EKE from altimetry is not reliable within a band of 5° on both sides of the equator due to geostrophic approximation.

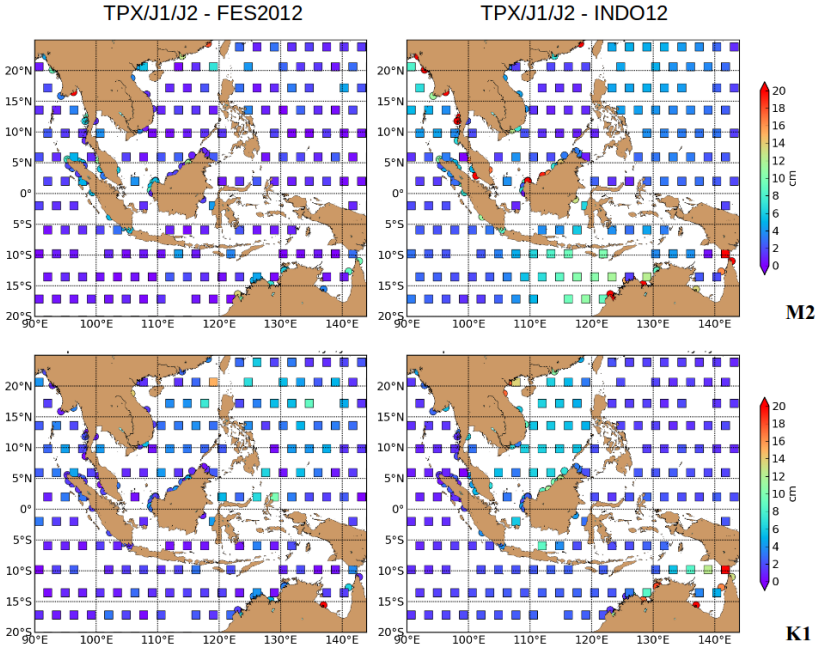

Figure 5. Surface tidal elevation complex differences at crossing points between TPX/J1/J2 and FES2012 (left) and INDO12 (right) symbolized by squares. Surface tidal elevation complex differences between tide gauges and FES2012 (left) and INDO12 (right) symbolized by circles. Units are in cm. M2 (top) and K1 (bottom) tidal components.

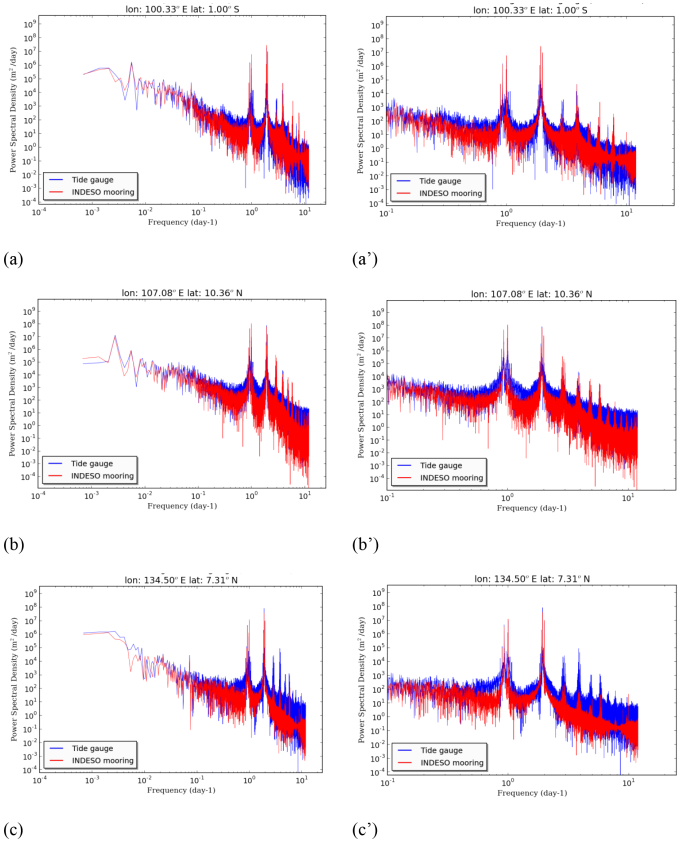

Figure 6. Power spectral density of the SSH for the model (red solid line) and for Tide gauges (blue solid line) at different locations (**a**: Padang (East-Sumatra), **b**: Vung Tau (SCS/South Vietnam) and **c**: Malakal (Pacific)) calculated during 2009–2012 period. Right panel is a zoom of the left panel.

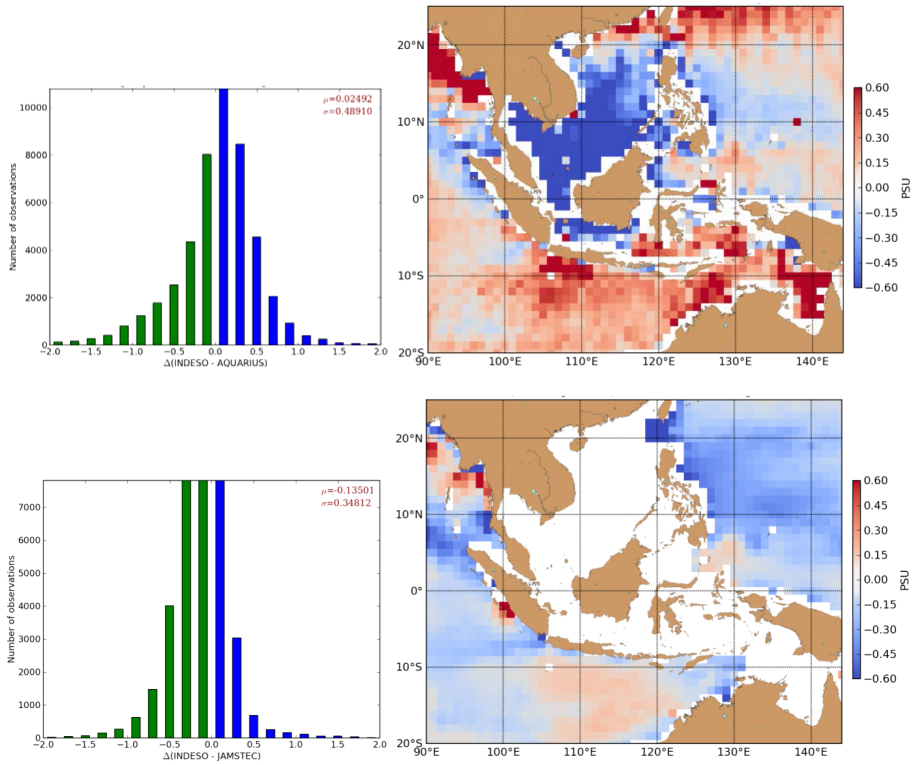

Figure 7. Mean bias (PSU) of the INDO12 SSS (monthly means) relative to Aquarius L3 (V3.0) (top) and JAMSTEC (ARGO+TRITON+CTD) (bottom) from August 2011 to December 2013.

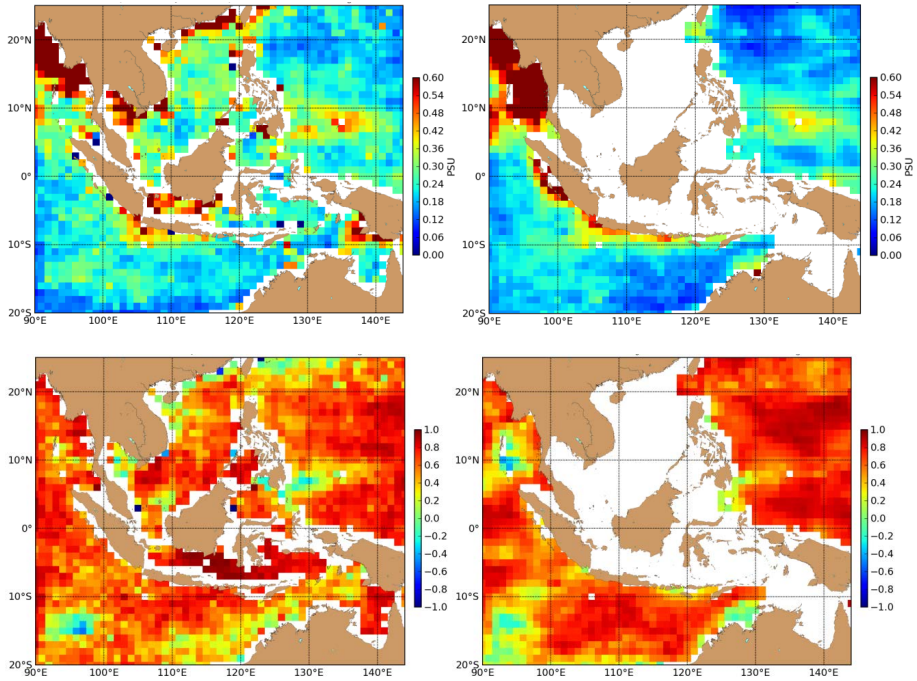

Figure 8. RMSD (top) and correlation (bottom) of INDO12 with respect to Aquarius (left) and JAMSTEC (ARGO+TRITON+CTD) (right) monthly map from August 2011 to December 2013.

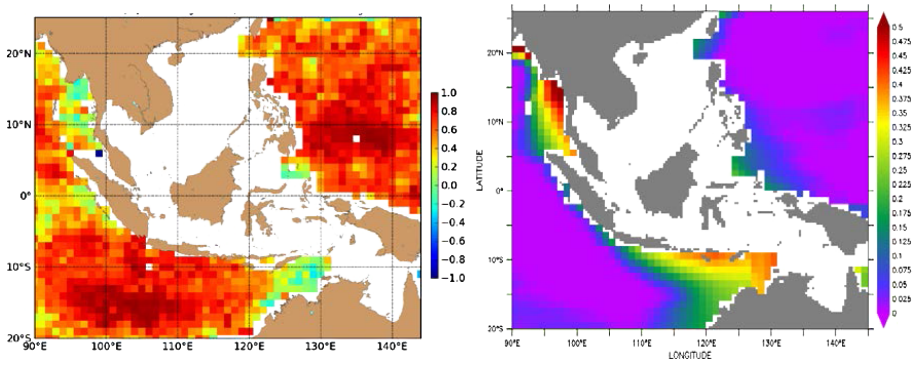

Figure 9. Mean temporal correlation between the (INDO12-Aquarius) SSS bias and the (INDO12-JAMSTEC) SSS bias and salinity interpolation error of JAMSTEC (ARGO+TRITON+CTD) calculated from August 2011 to December 2013.

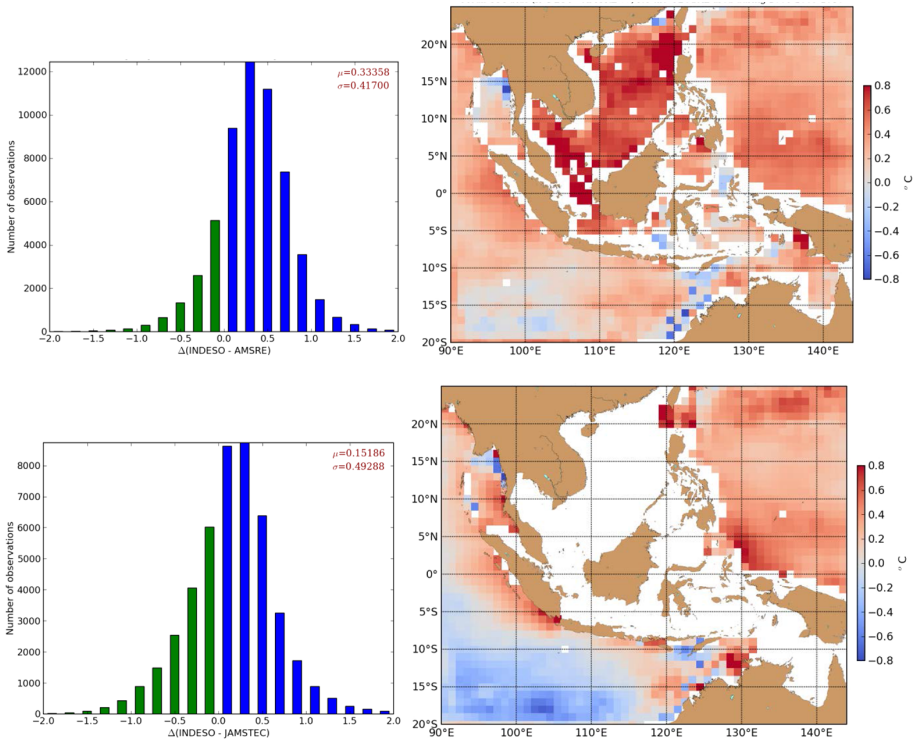

Figure 10. Mean bias (°C) of the INDO12 SST (monthly means) relative to AMSR-E (V7.0) (top) and JAMSTEC (ARGO+TRITON+CTD)) (bottom) for the years 2008–2010.

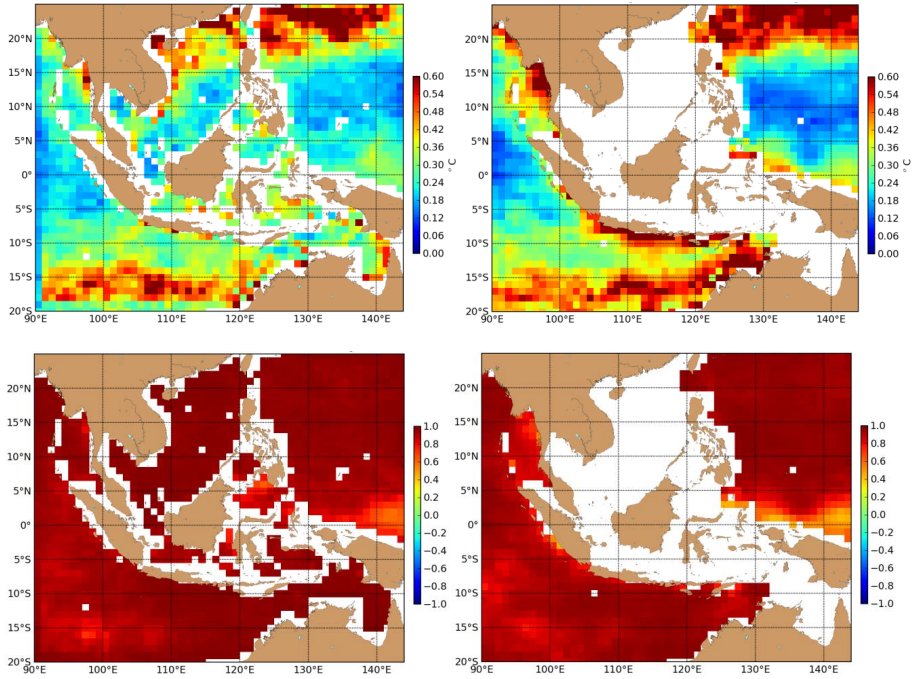

Figure 11. RMSD (top) and correlation (bottom) of INDO12 SST with respect to AMSR-E (left) and JAMSTEC (ARGO+TRITON+CTD) (right) calculated from monthly means (2008–2010).

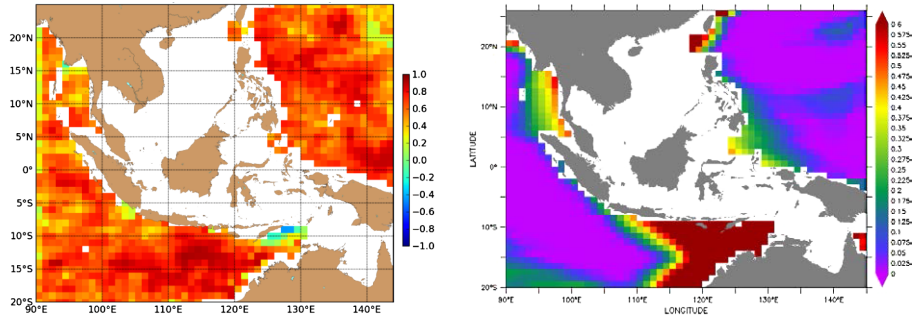

(a) (b)

Figure 12. Mean temporal correlation between the (INDO12-AMSR-E) SST bias and the (INDO12-JAMSTEC) SST bias **(a)** and temperature interpolation error of JAMSTEC (ARGO+TRITON+CTD) **(b)** calculated from 2008 to 2010.

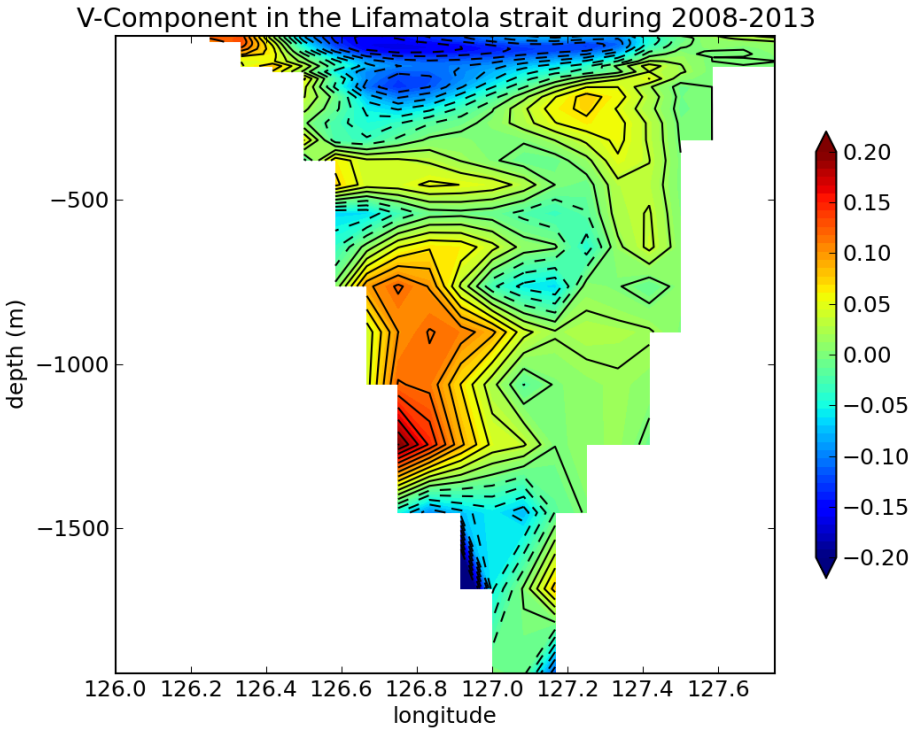

Figure 13. Mean of the along-strait velocity (m/s) in the Lifamatola Strait (2008–2013). Contour (dashed lines) means a negative value (Southward flow). Contour (solid lines) means a positive value (Northward flow).

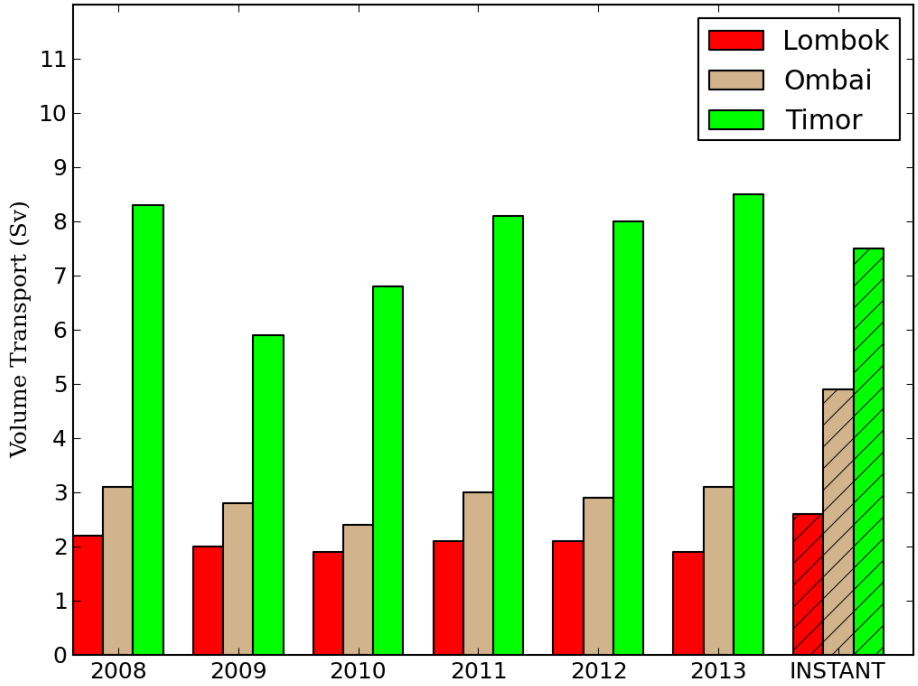

Figure 14. Model volume transport (Sv) into 3 main exits: Lombok (red), Ombaï (Brown), Timor (green) at different years. The Instant estimates (2004–2006) are shaded.

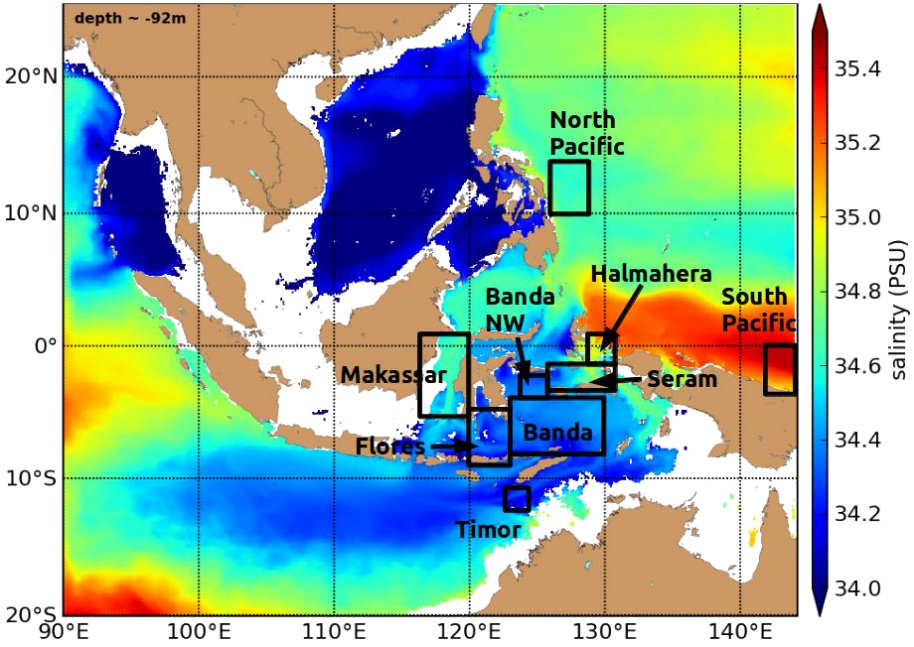

Figure 15. Main areas of water mass transformation. Color shading indicates salinity at 92 m depth.

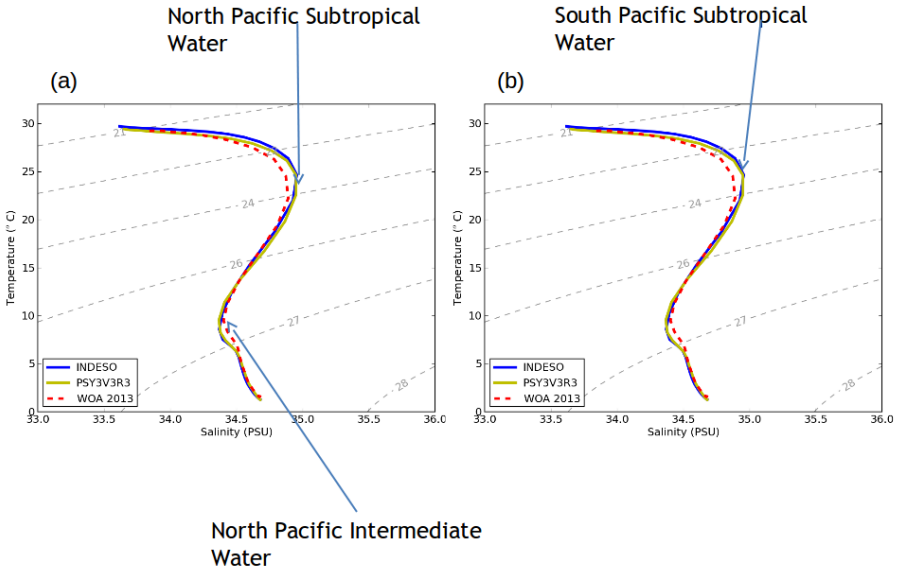

Figure 16. T/S diagrams from INDO12 simulation (green line) averaged on the Pacific North area **(a)** and the South Pacific area **(b)** and compared to climatologies WOA 2009 (dotted line) and PSY3V3R3 (yellow) in 2012. Salinity (PSU) and Temperature (°C) are plotted along x and y axes respectively.

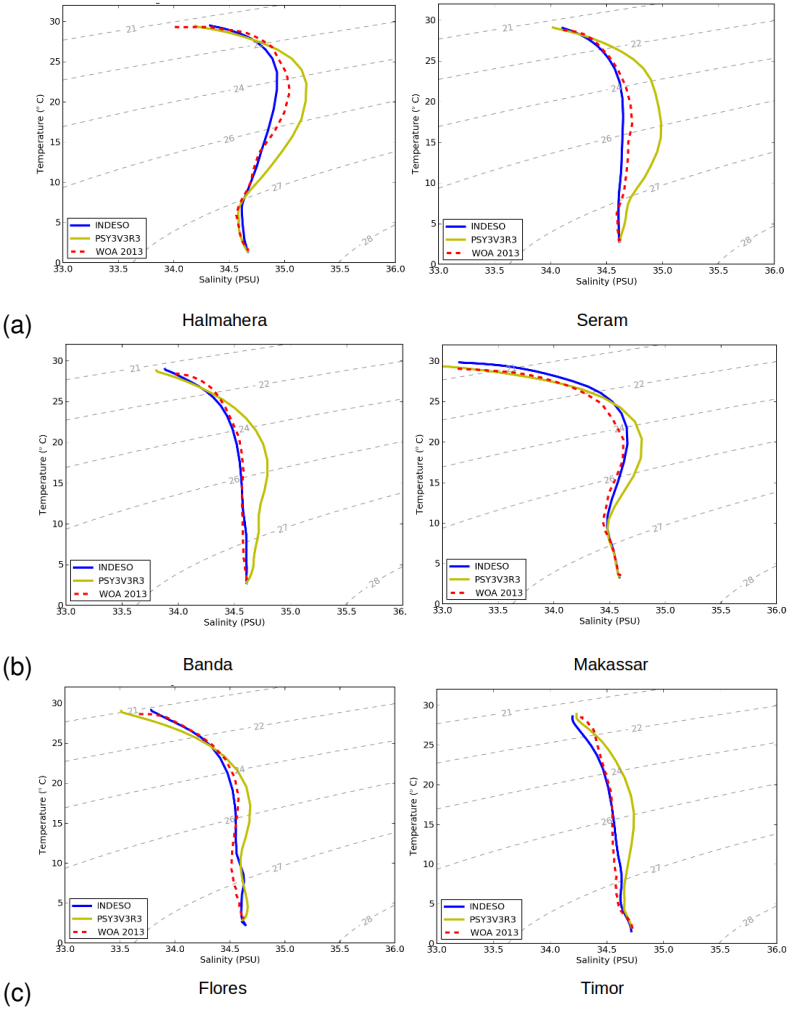
(a)
Halmahera
Seram
(b)
Banda
Makassar
(c)
Flores
Timor
Temperature (° C)
Salinity (PSU)
INDESO
PSY3V3R3
WOA 2013

Figure 17. T/S diagrams from INDO12 simulation (blue line) averaged on different areas, (a) Halmahera strait and Seram Sea, (b) Banda sea and Makassar Strait, (c) Flores Sea and Timor passage compared to climatologies WOA 2013 (red dotted line) and PSY3V3R3 (yellow line) for the 2008–2013 period. Salinity (PSU) and Temperature (°C) are plotted along x and y axes respectively.

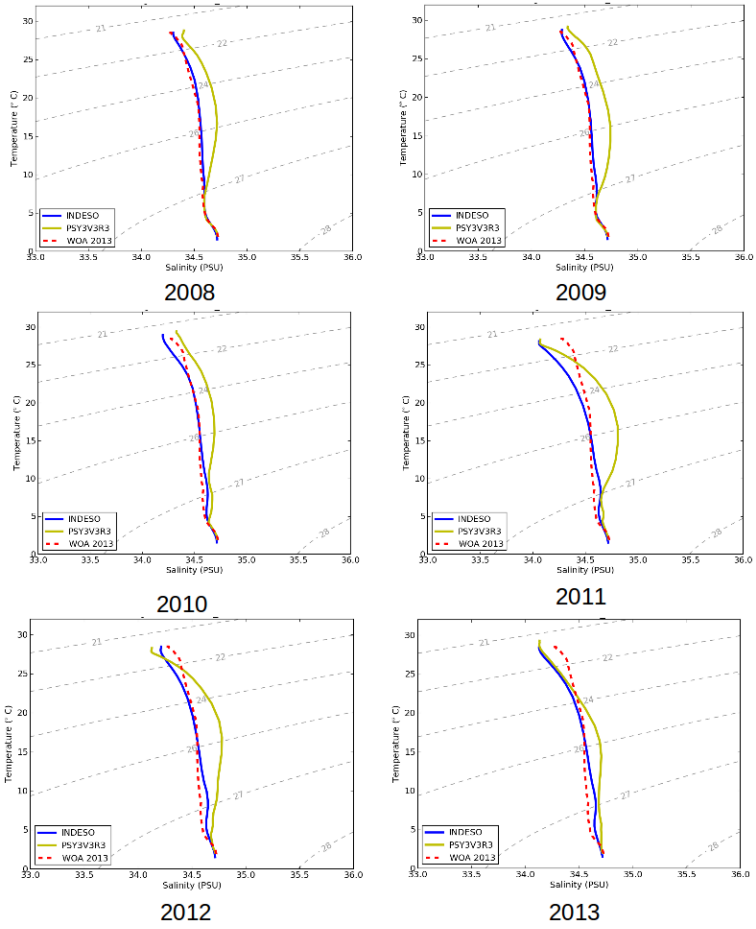

Figure 18. T/S diagrams from INDO12 simulation (blue line) averaged on the Timor region and compared to climatologies WOA 2013 (red dotted line) and PSY3V3R3 (yellow line) for years 2008 to 2013. Salinity (PSU) and Temperature (°C) are plotted along x and y axes respectively.

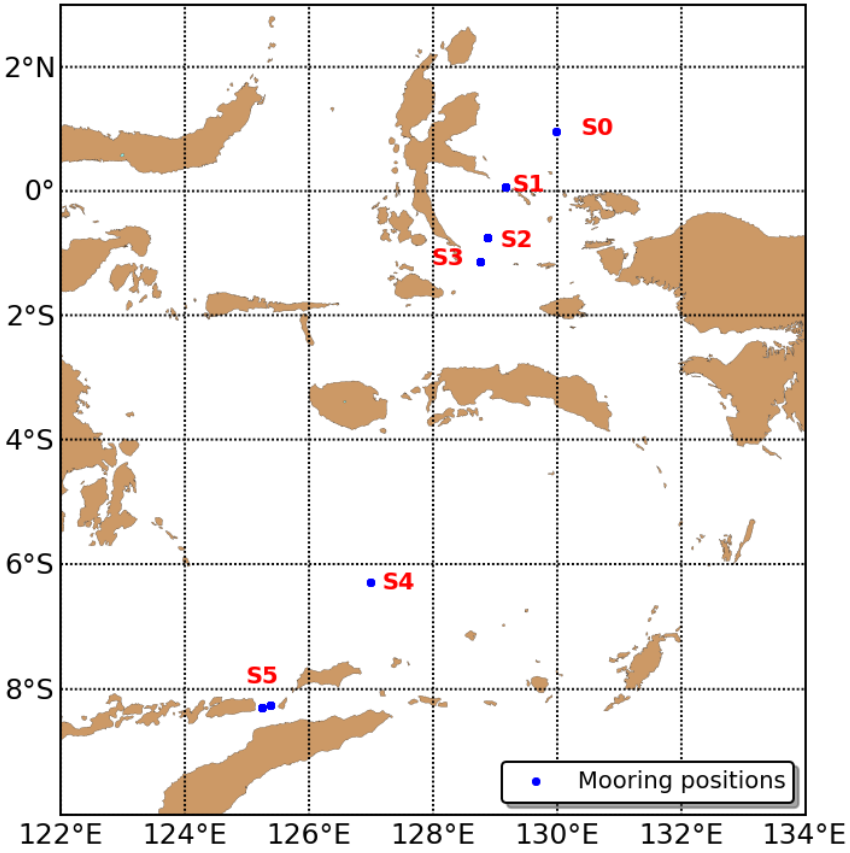

Figure 19. Locations of CTD moorings during the INDOMIX campaign (July 2010)

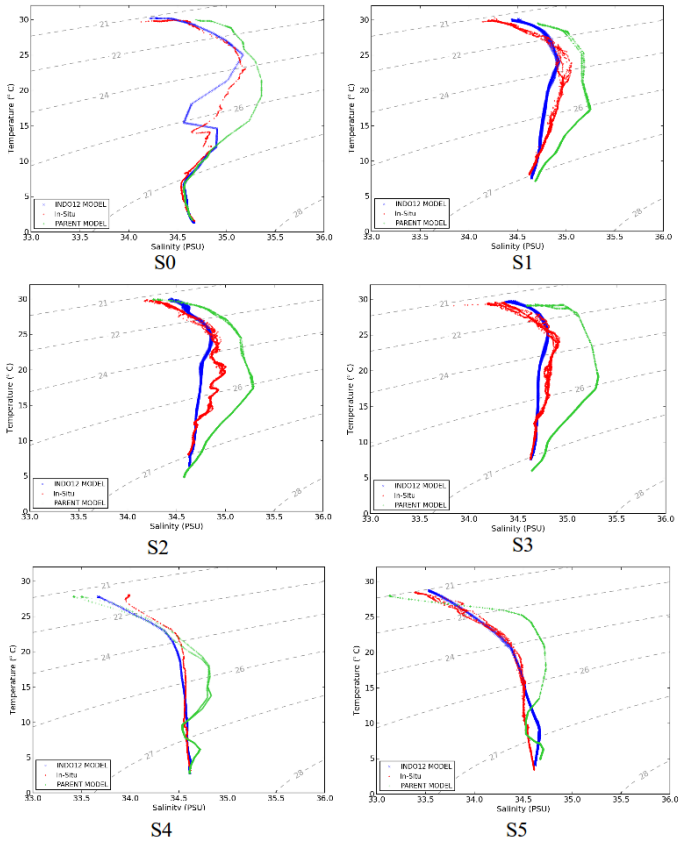

Figure 20. Collocated T/S diagrams to INDOMIX data (red) from hourly fields of INDO12 simulation (dark blue) and from daily mean fields of parent model PSY3 (green) in July 2010 at all mooring locations. Salinity (PSU) and Temperature (°C) are plotted along x and y axes respectively.

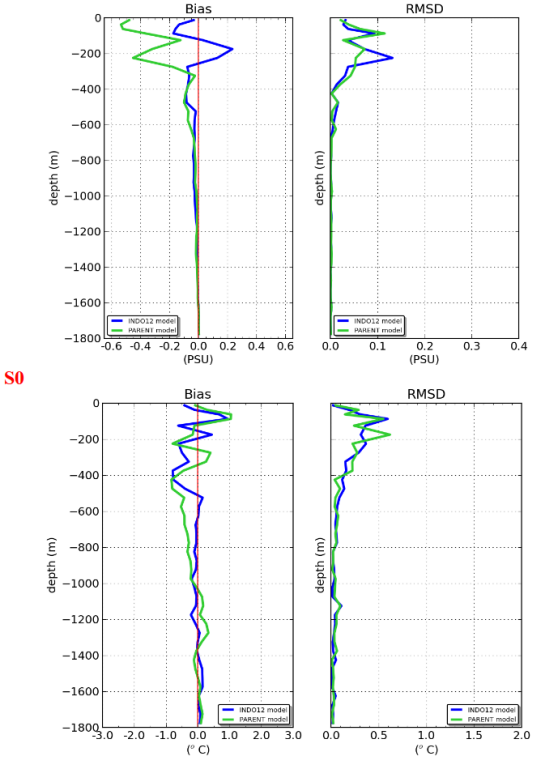

Figure 21a. Bias and RMSD of salinity (up) and temperature (bottom) between INDOMIX data and INDO12 (blue line) and parent model PSY3 (green line) at S0 location. Data are binned in 25m depth intervals for the first 100 meter depth and in 50 m depth interval for deeper layers.

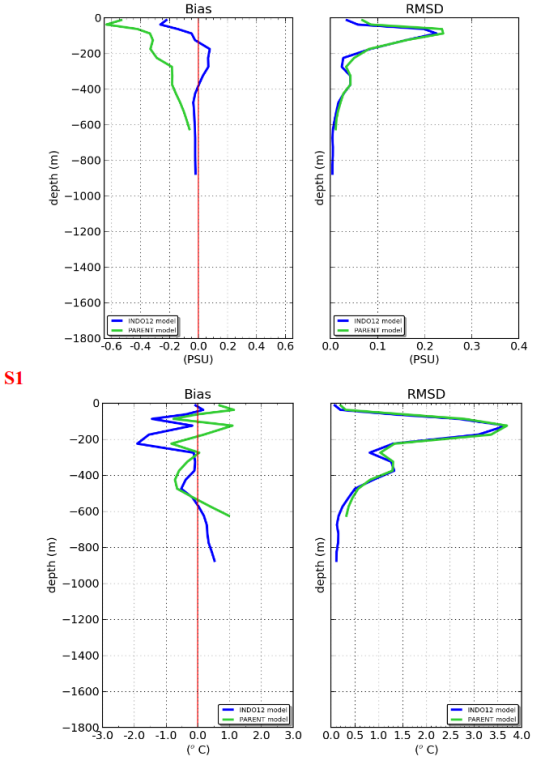

Figure 21b. Bias and RMSD of salinity (up) and temperature (bottom) between INDOMIX data and INDO12 (blue line) and parent model PSY3 (green line) at S1 location. Data are binned in 25m depth intervals for the first 100 meter depth and in 50 m depth interval for deeper layers.

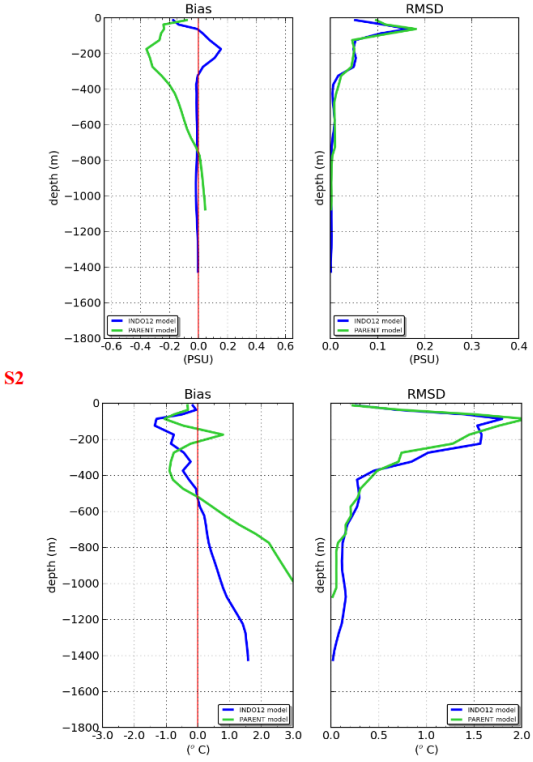

Figure 21c. Bias and RMSD of salinity (up) and temperature (bottom) between INDOMIX data and INDO12 (blue line) and parent model PSY3 (green line) at S2 location. Data are binned in 25m depth intervals for the first 100 meter depth and in 50 m depth interval for deeper layers.

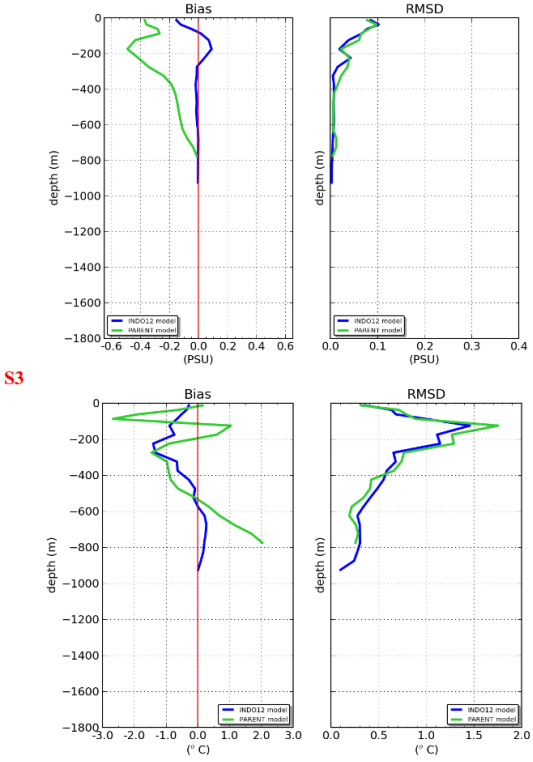

Figure 21d. Bias and RMSD of salinity (up) and temperature (bottom) between INDOMIX data and INDO12 (blue line) and parent model PSY3 (green line) at S3 location. Data are binned in 25m depth intervals for the first 100 meter depth and in 50 m depth interval for deeper layers.

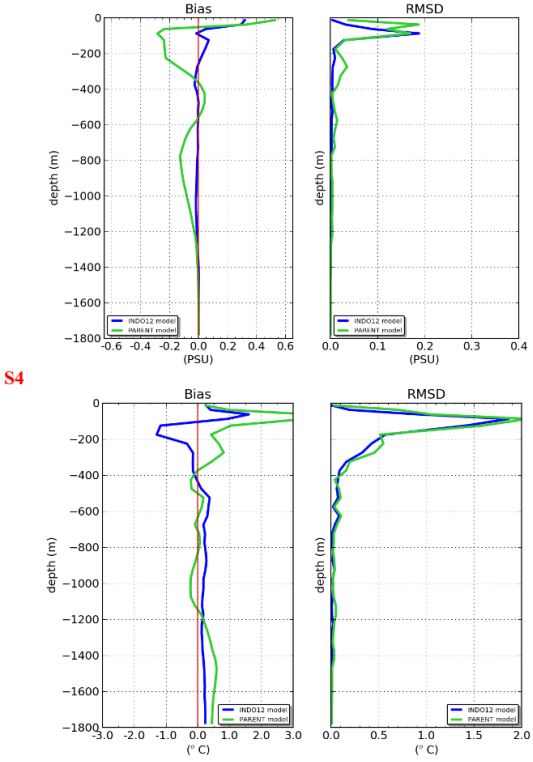

Figure 21e. Bias and RMSD of salinity (up) and temperature (bottom) between INDOMIX data and INDO12 (blue line) and parent model PSY3 (green line) at S4 location. Data are binned in 25m depth intervals for the first 100 meter depth and in 50 m depth interval for deeper layers.

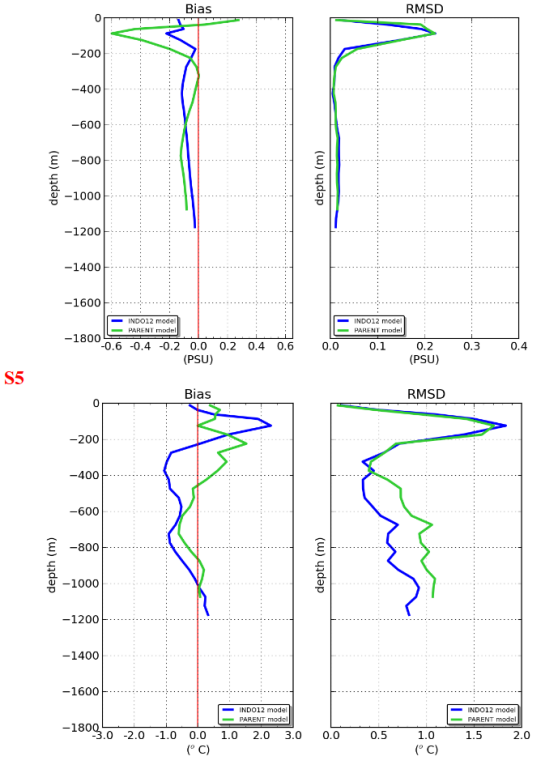

Figure 21f. Bias and RMSD of salinity (up) and temperature (bottom) between INDOMIX data and INDO12 (blue line) and parent model PSY3 (green line) at S5 location. Data are binned in 25m depth intervals for the first 100 meter depth and in 50 m depth interval for deeper layers.

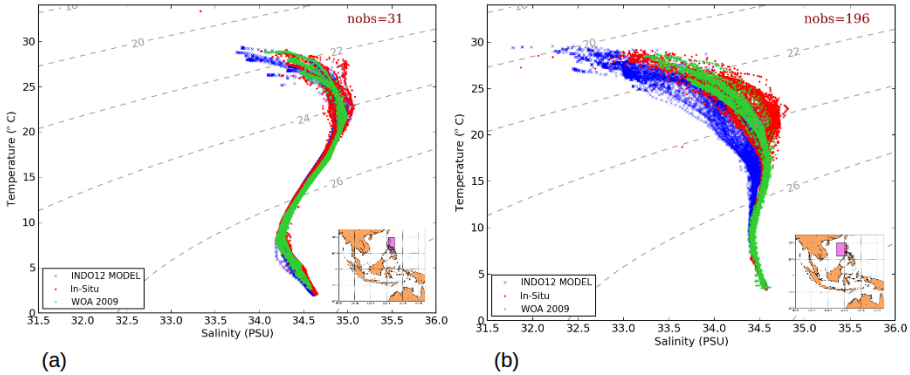

Figure 22. Collocated T–S diagrams to in-situ data (red) from INDO12 simulation (blue) and from climatology WOA2009 (green) on both sides of the Luzon strait (purple square) from October to December 2013. Salinity (PSU) and Temperature (°C) are plotted along x and y axes respectively.

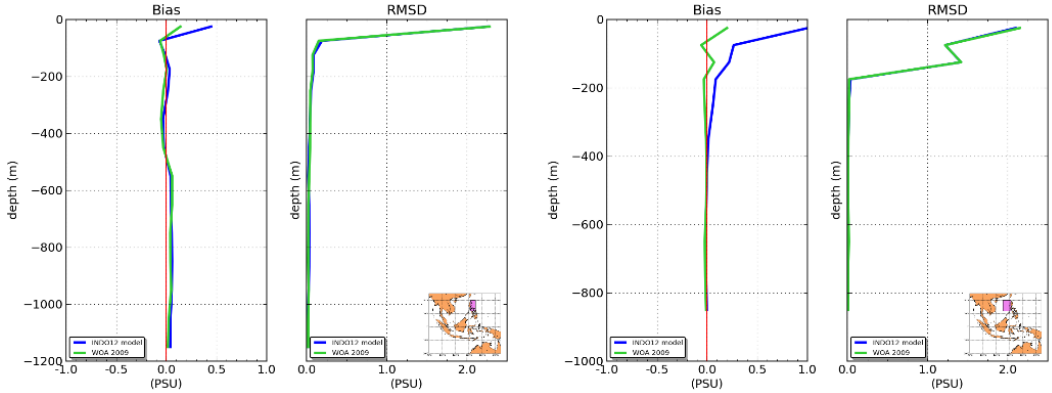

Figure 23a. Bias and RMSD of salinity between real data (WOD 2013) and INDO12 (blue) and WOA 2009 (green) on both sides of Luzon strait (purple squares) from October to December 2013. Data are binned in 50m depth intervals for the first 200 meter depths and in 100 m depth interval for deeper layers.

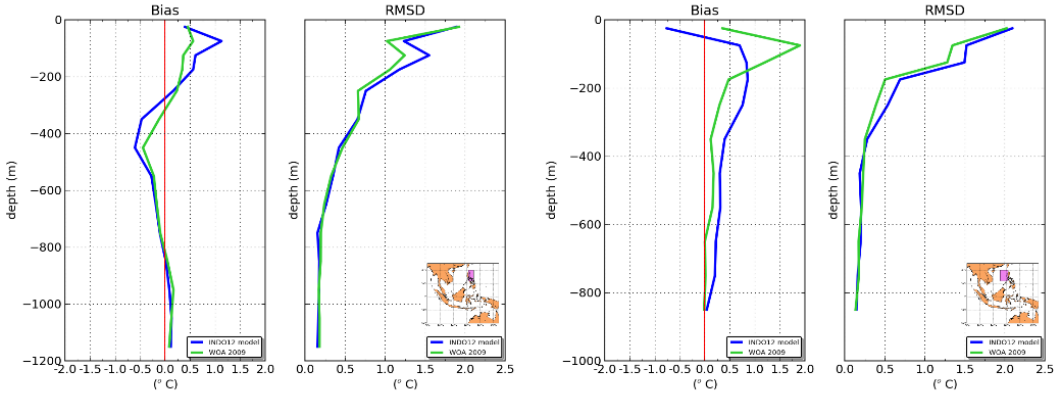

Figure 23b. Bias and RMSD of temperature between real data (WOD 2013) and INDO12 (blue) and WOA 2009 (green) on both sides of Luzon strait (purple squares) from October to December 2013. Data are binned in 50m depth intervals for the first 200 meter depths and in 100 m depth interval for deeper layers.